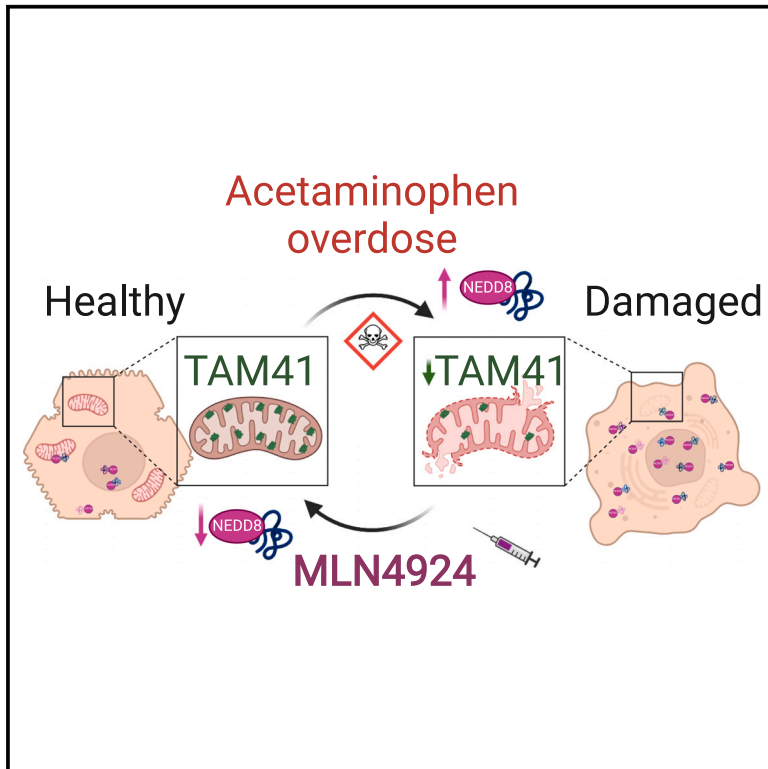


Neddylation inhibition prevents acetaminophen-induced liver damage by enhancing the anabolic cardiolipin pathway

Graphical abstract



Authors

Clàudia Gil-Pitarch,
Marina Serrano-Maciá, Jorge Simon, ...,
Naroa Goikoetxea-Usandizaga,
Irene González-Recio,
María L. Martínez-Chantar

Correspondence

irecio@cicbiogune.es (I.G.-R.),
mlmartinez@cicbiogune.es (M.L.M.-C.)

In brief

Gil-Pitarch et al. report that neddylation is significantly enriched during drug-induced liver injury (DILI), affecting mitochondrial dysfunction. MLN4924, a NEDD8-activating enzyme (NAE-1) inhibitor, decreases necrosis by promoting liver regeneration through the stabilization of TAM41 and mitochondrial recovery.

Highlights

- Hepatic NEDDylation levels are increased after drug liver injury
- NEDDylation inhibition (MLN4924) reduced necrosis and liver damage in mouse model
- TAM41 stability increases after MLN4924 treatment recovering cardiolipin synthesis
- A recovery of mitochondrial activity induces regeneration after MLN4924 treatment



Article

Neddylation inhibition prevents acetaminophen-induced liver damage by enhancing the anabolic cardiolipin pathway

Clàudia Gil-Pitarch,^{1,21} Marina Serrano-Maciá,^{1,21} Jorge Simon,¹ Laura Mosca,² Carolina Conter,¹ Claudia M. Rejano-Gordillo,^{1,3} L. Estefanía Zapata-Pavas,¹ Patricia Peña-Sanfélix,¹ Mikel Azkargorta,⁴ Rubén Rodríguez-Agudo,¹ Sofía Lachiondo-Ortega,¹ María Mercado-Gómez,¹ Teresa C. Delgado,¹ Marina Porcelli,² Igor Aurrekoetxea,^{5,6} James D. Sutherland,⁷ Rosa Barrio,⁷ Dimitris Xirodimas,⁸ Patricia Aspichueta,^{5,6,16} Felix Elortza,^{4,16}

(Author list continued on next page)

¹Liver Disease Lab, CIC bioGUNE, Basque Research and Technology Alliance, BRTA, Derio 48160 Bizkaia, Spain

²Department of Life Sciences, Health and Health Professions, Link University, Via del Casale di San Pio V, 44 00165 Rome, Italy

³Department of Biochemistry and Molecular Biology, Faculty of Sciences, University of Extremadura, University Institute of Biosanitary Research of Extremadura (INUBE), 06071 Badajoz, Spain

⁴Proteomics Platform, CIC bioGUNE, Basque Research and Technology Alliance (BRTA), ProteoRed-ISCI, CIBERehd, Science and Technology Park of Bizkaia, 48160 Derio, Spain

⁵Department of Physiology, Faculty of Medicine and Nursing, University of the Basque Country, UPV/EHU, 48940 Leioa, Spain

⁶BioBizkaia Health Research Institute, 48903 Barakaldo, Spain

⁷Center for Cooperative Research in Biosciences (CIC bioGUNE), Basque Research and Technology Alliance (BRTA), Bizkaia Technology Park, Building 801A, 48160 Derio, Spain

⁸CRBM, University Montpellier, CNRS, 34293 Montpellier, France

⁹Department of Physiology, School of Medicine-Instituto de Investigaciones Sanitarias, University of Santiago de Compostela, 15705 Santiago de Compostela, Spain

¹⁰Department of Physiology, CIMUS, 15782 University of Santiago de Compostela, Santiago de Compostela, Spain

¹¹CIBER Fisiopatología de la Obesidad y Nutrición (CIBERObn), Santiago de Compostela, Spain

¹²Galician Agency of Innovation (GAIN), Xunta de Galicia, Santiago de Compostela, Spain

¹³Gastroenterology and Hepatology Department, Marqués de Valdecilla University Hospital, Clinical and Translational Digestive Research Group, IDIVAL, 39011 Santander, Spain

¹⁴The Liver Unit, Newcastle-upon-Tyne Hospitals NHS Foundation Trust, NE7 7DN Newcastle upon Tyne, UK

(Affiliations continued on next page)

SUMMARY

Drug-induced liver injury (DILI) is a significant cause of acute liver failure (ALF) and liver transplantation in the Western world. Acetaminophen (APAP) overdose is a main contributor of DILI, leading to hepatocyte cell death through necrosis. Here, we identified that neddylation, an essential post-translational modification involved in the mitochondria function, was upregulated in liver biopsies from patients with APAP-induced liver injury (AILI) and in mice treated with an APAP overdose. MLN4924, an inhibitor of the neuronal precursor cell-expressed developmentally downregulated protein 8 (NEDD8)-activating enzyme (NAE-1), ameliorated necrosis and boosted liver regeneration in AILI. To understand how neddylation interferes in AILI, whole-body biotinylated NEDD8 (^{bio}NEDD8) and ubiquitin (^{bio}UB) transgenic mice were investigated under APAP overdose with and without MLN4924. The cytidine diphosphate diacylglycerol (CDP-DAG) synthase TAM41, responsible for producing cardiolipin essential for mitochondrial activity, was found modulated under AILI and restored its levels by inhibiting neddylation. Understanding this ubiquitin-like crosstalk in AILI is essential for developing promising targeted inhibitors for DILI treatment.

INTRODUCTION

In the Western world, drug-induced liver injury (DILI) is the leading cause of acute liver failure (ALF) and liver transplantation. It has become a major public health problem, affecting 19 out of

every 100,000 people worldwide.¹ Importantly, paracetamol, also known as acetaminophen or APAP, is the leading cause of ALF in the United States (46%) and accounts for 40% to 70% of cases in the United Kingdom and Europe.² Every year, APAP is responsible for 500 DILI deaths, 100,000 calls to the



Luis Alfonso Martínez-Cruz,¹ Rubén Nogueiras,^{9,10,11,12} Paula Iruzubieta,¹³ Javier Crespo,¹³ Steven Masson,^{14,15} Misti Vanette McCain,¹⁵ Helen L. Reeves,^{14,15} Raul J. Andrade,^{16,17} M. Isabel Lucena,^{16,18} Ugo Mayor,^{19,20} Naroa Goikoetxea-Usandizaga,^{1,16} Irene González-Recio,^{1,22,*} and María L. Martínez-Chantar^{1,16,22,23,*}

¹⁵Newcastle University Translational and Clinical Research Institute, The Medical School, Newcastle University, NE2 4HH Newcastle upon Tyne, UK

¹⁶Centro de Investigación Biomédica en Red de Enfermedades Hepáticas y Digestivas (CIBERehd), Carlos III National Health Institute, 28029 Madrid, Spain

¹⁷Unidad de Gestión Clínica de Enfermedades Digestivas, Instituto de Investigación Biomédica de Málaga-IBIMA, Hospital Universitario Virgen de la Victoria, Universidad de Málaga, 29590 Málaga, Spain

¹⁸Servicio de Farmacología Clínica, Instituto de Investigación Biomédica de Málaga-IBIMA, Hospital Universitario Virgen de la Victoria, UICEC SCReN, Universidad de Málaga, 29590 Málaga, Spain

¹⁹Department of Biochemistry and Molecular Biology, Faculty of Science and Technology, University of the Basque Country (UPV/EHU), 48940 Leioa, Spain

²⁰Kerbasque, Basque Foundation for Science, 48013 Bilbao, Spain

²¹These authors contributed equally

²²Senior author

²³Lead contact

*Correspondence: irecio@cicbiogune.es (I.G.-R.), mlmartinez@cicbiogune.es (M.L.M.-C.)

<https://doi.org/10.1016/j.xcrm.2024.101653>

US Poison Center, 50,000 emergency room visits, and 10,000 hospitalizations in the United States.³

Nowadays, N-acetylcysteine, a scavenger of reactive oxygen species (ROS), is the only approved pharmacological treatment for hepatotoxicity due to APAP overdose. However, due to the narrow therapeutic window and rapid disease progression, the therapeutic efficacy of N-acetylcysteine is still limited.⁴ For patients at the advanced stage, liver transplantation is the only way to improve survival outcomes. Therefore, new therapeutic approaches are required in this field.⁵

Previous studies have shown that APAP overdose leads to mitochondrial dysfunction via several mechanisms, including inhibition of several mitochondrial respiratory chain complexes by the reactive metabolite N-acetyl-*p*-benzoquinoneimine and possibly some components of mitochondrial fatty acid oxidation metabolism and mitochondrial DNA depletion.⁶ High APAP concentrations had no effect on complex III, IV, or V but decreased the mitochondrial respiratory capacity of complex I and II in human liver.⁵ In addition, N-acetyl-*p*-benzoquinone imine (NAPQI) leads to depletion of glutathione (GSH) in liver cells, which has significant effects on protein function and mitochondrial redox state. Since GSH serves as the primary intracellular antioxidant, its depletion leads to ROS production.

In eukaryotes, protein neddylation is an important ubiquitin-like post-translational modification (PTM).⁷ To date, neddylation has been widely used to tag conserved neuronal precursor cell-expressed developmentally downregulated protein 8 (NEDD8) onto substrates to modulate activity and cellular localization.⁶ The cullin-RING E3 ubiquitin ligases (CRLs) were the first well-known NEDDylation target.⁸ This protein family has a conserved NEDDylation site and requires NEDD8 covalent attachment to induce a conformational change in the structure that activates ubiquitin ligation to substrates.⁹ Several studies have found that CRLs play an active role in the regulation of morphology, trafficking, functions, and mitochondrial degradation, with the ubiquitination protein system being primarily involved in the degradation of the mitochondrial compartment's outer membrane.⁶ Indeed, selective inhibition of CRL3 provides protection from liver damage induced by APAP in mice.¹⁰

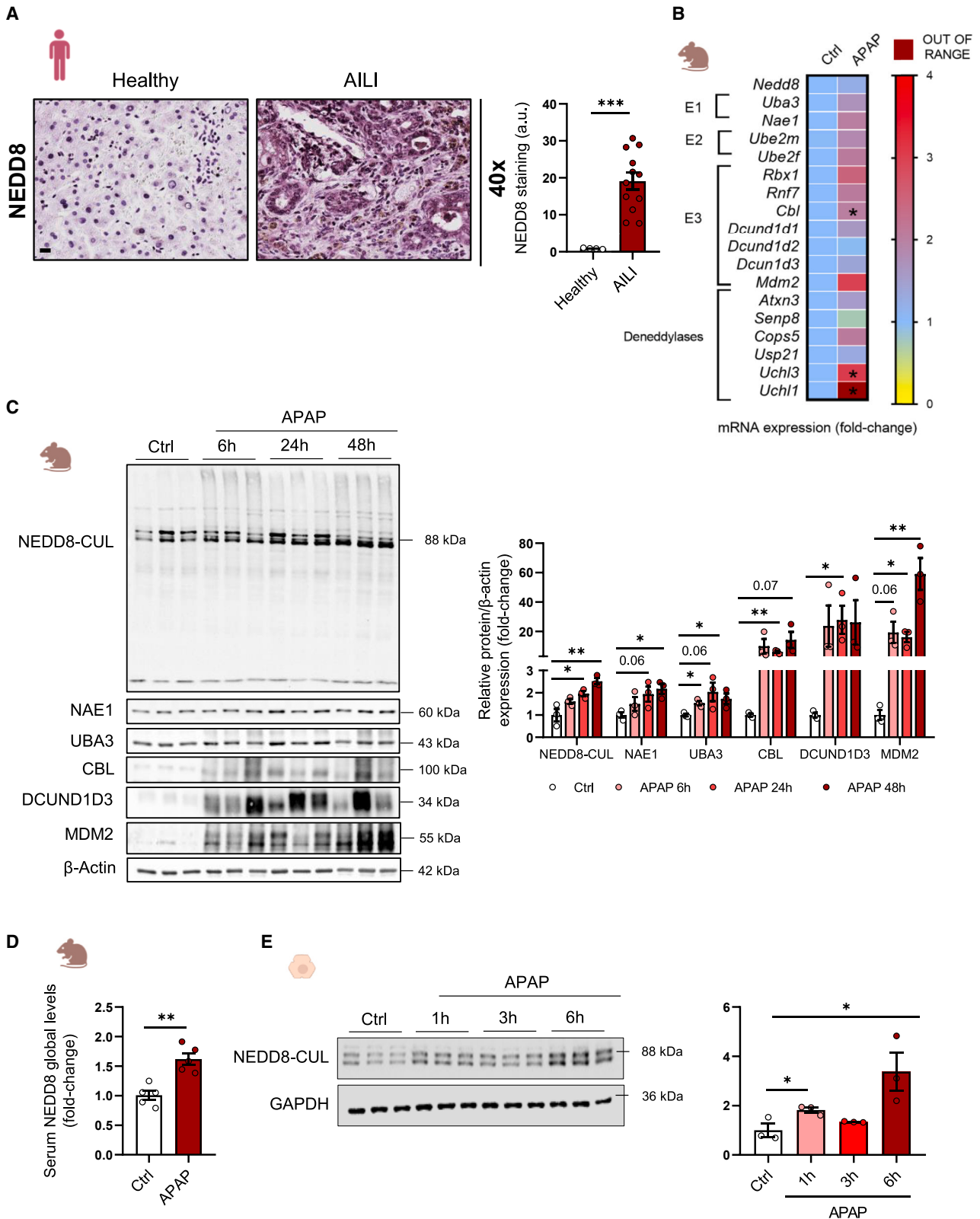
MLN4924 (also known as pevonedistat) is a small molecular inhibitor of the catalytic subunit of the NEDD8-activating enzyme (NAE-1), blocking the entire neddylation modification and inactivating all CRLs. The outcomes after blocking neddylation in mitochondrial function appear to vary depending on cell type. Some studies point out that MLN4924 induces oxidative stress and promotes autophagy in a variety of malignant cells,¹¹ whereas our group and others have demonstrated that this inhibitor blocks ROS in non-alcoholic fatty liver disease (NAFLD)¹² or suppresses basal but not maximal oxidative phosphorylation in pro-tumoral hepatocytes.¹³

Considering that the role of neddylation in liver pathology has raised significant expectations,^{12,14,15} we investigated the impact of neddylation in response to the damage caused by APAP overdose. Neddylation was found to be overrepresented in the liver biopsies from patients with AILI (APAP-induced liver injury) and in preclinical studies that resemble this pathology. Indeed, inhibiting NEDD8 conjugation with MLN4924 in animal models under APAP overdose resulted in a halt in liver injury and an increase in hepatic regeneration. The hepatic neddylation and ubiquitome were further characterized employing biotinylated ubiquitin (^{bio}UB) and biotinylated NEDD8 (^{bio}NEDD8) transgenic mice under APAP overdose model in the presence or absence of MLN4924. The findings revealed that the cytidine diphosphate diacylglycerol (CDP-DAG) synthase TAM41 was overexpressed in the AILI model when neddylation was inhibited, resulting in high levels of cardiolipin (CL), which is required for optimal mitochondrial function.¹⁶ Thus, neddylation inhibition halts AILI boosting anabolic cardiolipin pathway.

RESULTS

Alteration of NEDD8-protein homeostasis in patients with AILI and in preclinical models of hepatotoxicity by APAP overdose

DILI is a complex liver pathology characterized by massive ROS production as well as inflammatory and necrotic processes in response to APAP overdose.¹⁷ Disruptions in the NEDD8 proteome have been linked to oxidative stress-related liver



(legend on next page)

pathologies.^{12,15,18} Thus, the amount of free NEDD8 and NEDD8-conjugated proteins was assessed in liver samples from patients with AILI to ascertain whether abnormal neddylation appears dysregulated in APAP-associated liver damage. Comparing patients with AILI to healthy controls, a quantitative histological examination showed an increase in the liver neddylation proteome (Figure 1A; Table S1).

The use of preclinical mouse models, mimicking APAP overdose in patients with AILI, has revealed key insights into the pathology. Gene expression assays highlighted significant alterations in the neddylation cycle in the livers of the animal model treated with the hepatotoxic compound¹⁹ (Figure 1B). These findings were supported by western blot analyses, at 6, 24, and 48 h of APAP damage, which demonstrated an early-stage increase in neddylation profiles and in the E1 and E3 enzymes (Figure 1C). Moreover, serum samples from the animal models further validated the rise in neddylation proteins post-APAP overdose (Figure 1D).

Primary hepatocytes exposed to a toxic APAP dose (10 mM) also exhibited a pronounced increase in neddylation cullins (Figure 1E), indicating a clear association between aberrant neddylation and hepatic damage.

Collectively, these findings underscore the critical role of atypical neddylation in the context of liver injury in both human AILI cases and animal models.

Inhibition of neddylation resolves APAP toxicity in mice

To gain insight into the functional consequences that neddylation has in the liver of patients with AILI and in mice under a toxic dose of APAP, we inhibited the NEDD8-conjugated activity with the NAE-1 inhibitor MLN4924 in the preclinical mice model under APAP-induced toxicity. Twenty-four hours after APAP administration, these mice received MLN4924 in a single dose (Figure S1A). Mice were sacrificed 24 h after MLN4924 treatment, and the effect was confirmed by immunohistochemistry (IHC) and western blot analyses of the NEDD8 proteome in these mice (Figures 2A and S1B). Animals treated with MLN4924 under APAP overdose presented a significant reduction of neddylation proteins in comparison to the liver of non-treated mice and exposure to the hepatotoxic compound (Figure 2A). The image quantification at a higher magnification is shown in Figure S1C. In line with these results, H&E staining and TUNEL assay revealed the presence of necrotic areas in the APAP-treated mice, which were significantly reduced with MLN4924 treatment (Figures 2B and 2C). Inflammatory response is a well-known process during DILI.¹⁹ Analysis of macrophage F4/80 staining reveals a lower number of Kupffer cells under NAE-1 inhibition (Figure 2D). The

image quantification at a higher magnification is shown in Figure S1C. Consistently, the levels of tumor necrosis factor and interleukin-6 were measured in the serum of these animal models (Figure 2E). Inhibiting neddylation significantly reduced the levels of both cytokines as well as the serum transaminases (Figures 2E and 2F).

To assess the influence of neddylation inhibition on inflammatory responses, a new preclinical study was performed. Mice were administered MLN4924 shortly after the induction of hepatic damage, precisely 6 h following an APAP overdose, as depicted in Figure S2A. Subsequent evaluation at 18 h post-treatment revealed a marked decrease in necrotic areas and TUNEL-positive staining in the treated animals (Figure S2A). Concurrently, there was a notable attenuation of the inflammatory process, as evidenced by a significant reduction in F4/80 staining (Figure S2A). This reduction was also correlated with decreased transaminase levels, indicating a mitigation of liver injury (Figure S2B).

The outcomes revealed that MLN4924 treatment leads to a significant decrease of NEDD8 levels, which is closely linked with a reversal of the principal characteristics of DILI, including necrosis and inflammatory processes.

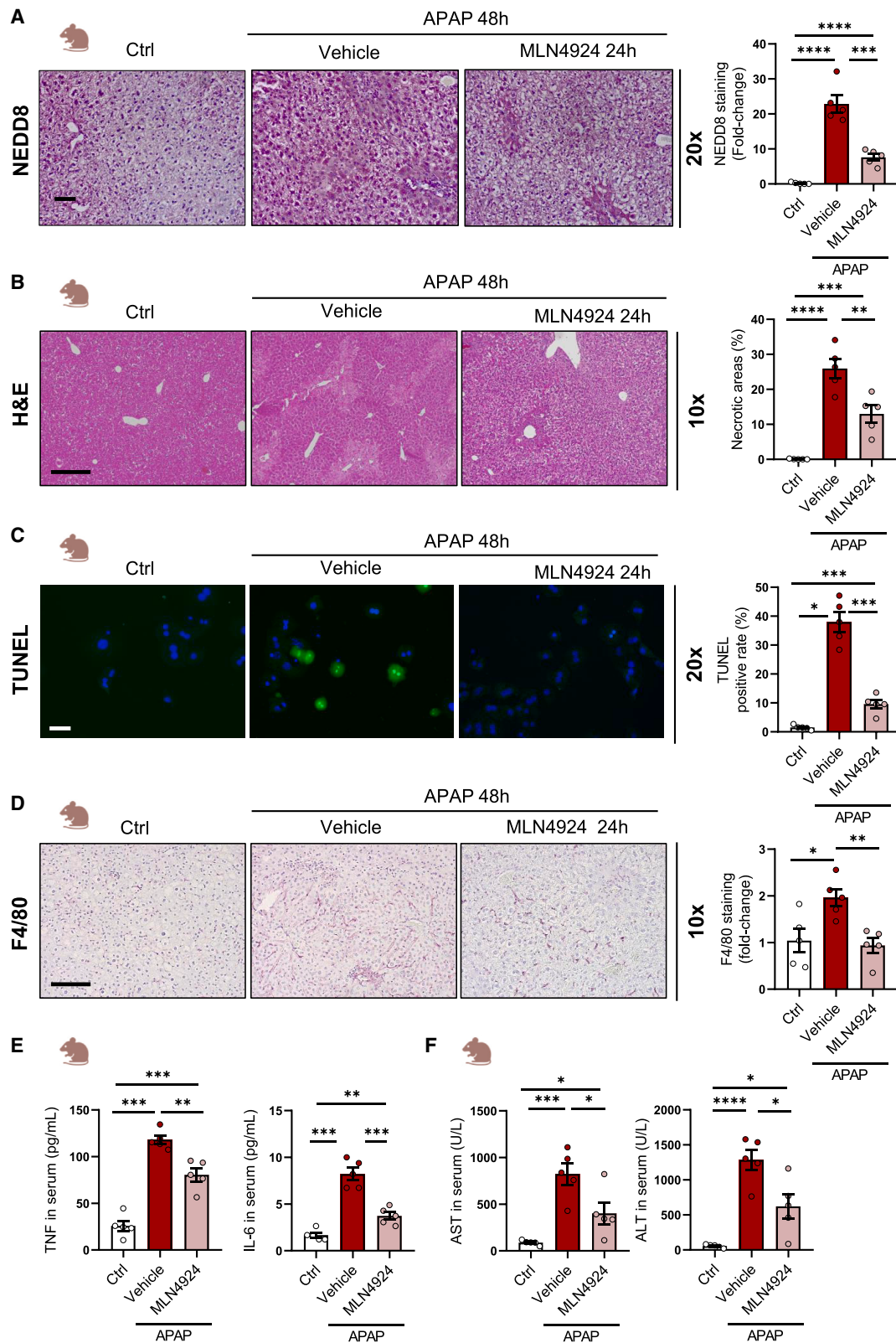
Proteomic insights into the APAP mouse model treated with neddylation inhibition drug

The CRLs family are well-known NEDD8 substrates.¹² Cullin neddylation causes a conformational change in the E3 ubiquitin ligases, increasing their activity over their substrates, which is typically ubiquitination for protein degradation.¹⁴ Other non-cullin NEDD8 substrates, including p53, HuR, LKB1, and Akt, have been found to be regulated in stability, localization, and function for this PTM.^{13,20,21} As a result, neddylation regulates multiple molecular pathways at the same time.²² The landscape of hepatic neddylation proteins under the pathological condition of AILI was then delineated to elucidate how APAP toxicity affects this PTM. For that purpose, we employed whole-body genetically modified mice that express a ^{bio}NEDD8 construct (Figure S3A), which do not show any alteration in necrotic areas or the serum markers compared to wild-type (WT) mice (Figures S3B and S3C). Furthermore, when genes associated with APAP metabolism and oxidative stress were examined, no significant changes were observed in either animal model (Figure S3D). Similarly, analysis of the neddylation profile revealed no discernible alterations (Figure S3E).

Biotin pull-down experiments were then performed in ^{bio}NEDD8 mice to see how the hepatic biotin-neddylation proteome is modulated following 24 h of APAP with/without MLN4924. The volcano plot analysis of the hepatic neddylation

Figure 1. Global NEDD8 is characterized in patients with AILI and in preclinical mice models with an APAP overdose

(A) Liver immunohistochemical staining and respective quantification of NEDD8 in a cohort of patients with AILI ($N = 12$) compared to a healthy group ($n = 4$). Scale bar corresponds to 50 μm .
 (B) mRNA expression levels of NEDD8 pathway (*Nedd8*, *Uba3*, *Nae-1*, *Ube2m*, *Ube2f*, *Rbx1*, *Rnf7*, *Cbl*, *Dcund1d1*, *Dcund1d2*, *Dcun1d3*, *Mdm2*, *Atxn3*, *Senp8*, *Cops5*, *Usp21*, *Uchl3*, and *Uchl1*) in mice treated with 360 mg/kg of APAP ($n = 4$) for 48 h and compared with a control group ($n = 4$).
 (C) Protein expression levels of NEDD8 and the enzymes involved in the NEDDylation pathway NAE-1, UBA3, CBL, DCUN1D3, and MDM2 in liver from mice treated with a single dose of 360 mg/kg of APAP ($n = 3$) for 6, 24, and 48 h and compared with a control group ($n = 3$). β -Actin was used as a loading control.
 (D) NEDD8 serum levels was determined in APAP overdose mice models ($n = 5$) for 48 h and compared to a control group ($n = 5$).
 (E) Protein expression levels of NEDD8 in primary hepatocytes treated with 10 mM of APAP overdose for 1, 3, and 6 h. GAPDH was used as a loading control. Triplicates were used for experimental condition. Data are shown as mean \pm SEM. * $p < 0.05$, ** $p < 0.01$, and *** $p < 0.001$ are shown (Student's test).



(legend on next page)

because of the APAP response in comparison to the control group revealed the proteins that were significantly modulated, as shown in Figure S3F. Furthermore, “the Database for Annotation, Visualization, and Integrated Discovery” (DAVID) (<https://david.ncifcrf.gov/>) analysis showed biological processes such as peroxide catabolism and natural killer cell-mediated toxicity, which could be linked to reactive oxygen production and the inflammatory response seen in AILI (Figure S3G). Further investigation revealed that peroxidase activity was also significantly represented in molecular function (Figure S3G).

In these ^{bio}NEDD8 mice, MLN4924 effects were represented in a volcano plot (Figure 3A), and the analysis performed by the DAVID analysis identified the overrepresented biological processes, which included processes related to response to oxidative stress; for instance, TAM41, a CDP-DAG synthase required for cardiolipin biosynthesis in mitochondria.¹⁶ Functional enrichment analysis of differentially neddylation proteins showed molecular function associated with cellular iron homeostasis (Figure 3B). These findings support previous research indicating the importance of cardiolipin in maintaining mitochondrial and cellular iron homeostasis.²³

Western blot from the liver of APAP or APAP plus MLN4924 versus WT mice showed a TAM41 upregulation, while in the mice treated with APAP, the levels of this protein were significantly diminished (Figure 3C).

To better understand how neddylation affects TAM41 levels, we mapped the ubiquitinated proteome after APAP damage. For this, we used transgenic mice that expressed whole-body ^{bio}UB (Figure S3A). The phenotype of these animals was comparable to that of the WT.²⁴ To isolate the hepatic biotin-ubiquitin proteome, ^{bio}UB mice were treated with APAP in the presence or absence of MLN4924 and sacrificed 48 h after APAP overdose (Figure 3D). In these experimental circumstances, the western blot against TAM41 demonstrated that ubiquitinated forms of this protein occur in control mice and in the group that received APAP and MLN4924 treatments, which corresponds to inhibition in the neddylation of cullins (Figure 3D). To further corroborate these data, immunoprecipitation assays targeting NEDD8 were conducted, and the concentrations of TAM41 were quantified within these extracts. It was observed that TAM41 levels tended to diminish following APAP administration. However, this reduction was significantly abrogated upon treatment with MLN4924, indicating its potential in reversing the effects of APAP (Figures 3E and S3H).

To enhance our understanding of TAM41’s regulatory mechanisms in a cellular context, we treated primary hepatocytes with the translational inhibitor cycloheximide, either alone or in combination with the proteasome inhibitor MG132 and the neddylation

inhibitor MLN4924. This approach builds on previous observations that indicated TAM41 undergoes both neddylation and ubiquitination. It was found that a 12-h inhibition of protein synthesis by cycloheximide increases TAM41 stability, suggesting a protective effect against degradation pathways. Interestingly, when MG132 was applied, it not only confirmed this protective effect but also accelerated the stabilization process, observable at just 8 h. In a parallel finding, the introduction of MLN4924 during the early phase of treatment raised TAM41 protein levels (Figure S3I).

Finally, in line with these results, we found that the levels of cardiolipin in the livers from WT mice treated with APAP plus MLN4924 were significantly upregulated as compared to the experimental group without MLN4924 therapy (Figure 3F).

Cytochrome c oxidase is the terminal complex of eukaryotic oxidative phosphorylation in mitochondria. The electrochemical gradient formed during the process is used to generate chemical energy in the form of ATP to power vital cellular processes.²⁵ It has already been reported that the identification of cardiolipin-binding sites on cytochrome c oxidase at the entrance of proton channels modulates its activity.²⁶ Regarding the role of cardiolipin in cytochrome c oxidase, our findings show that in isolated membranes, blocking neddylation in primary hepatocytes treated with APAP restores its activity in comparison to untreated cells (Figure 3G). These findings highlighted the significance of increasing TAM41 levels in the presence of NAE-1 inhibitor MLN4924, inducing cardiolipin levels, and modulating cytochrome c oxidase activity, which could maintain oxidative phosphorylation in mitochondria.

Targeting neddylation reduces mitochondrial dysfunction in the liver under APAP overdose

Mitochondrial dysfunction is one of the main hallmarks of liver injury triggered by APAP intoxication,¹⁷ and its recovered function has been described as a potential therapy to improve liver regeneration after damage induction.^{27,28}

In line with the proteomic analysis conducted on preclinical APAP models revealing significant impairment of mitochondrial function due to neddylation, the TUNEL assay demonstrated a marked reduction in apoptotic response in hepatocytes treated with MLN4924 compared to those treated solely with APAP (Figure 4A). Moreover, MLN4924 treatment substantially elevated active mitochondrial levels, as demonstrated by MitoTracker measurements, while concomitantly resulting in a marked reduction in ROS production, as determined by MitoSOX analysis (Figure 4A). These results collectively imply a promising therapeutic potential for MLN4924 in ameliorating

Figure 2. Pharmacological neddylation inhibition reduces liver damage

Comparison of control mice ($n = 5$) versus mice treated with 360 mg/kg of APAP overdose ($n = 5$) versus with 360 mg/kg of APAP overdose and 24 h later with 60 mg/kg MLN4924 ($n = 5$).

(A) Liver immunohistochemical staining and respective quantification of NEDD8 ($n = 5$). Scale bar corresponds to 100 μ m.

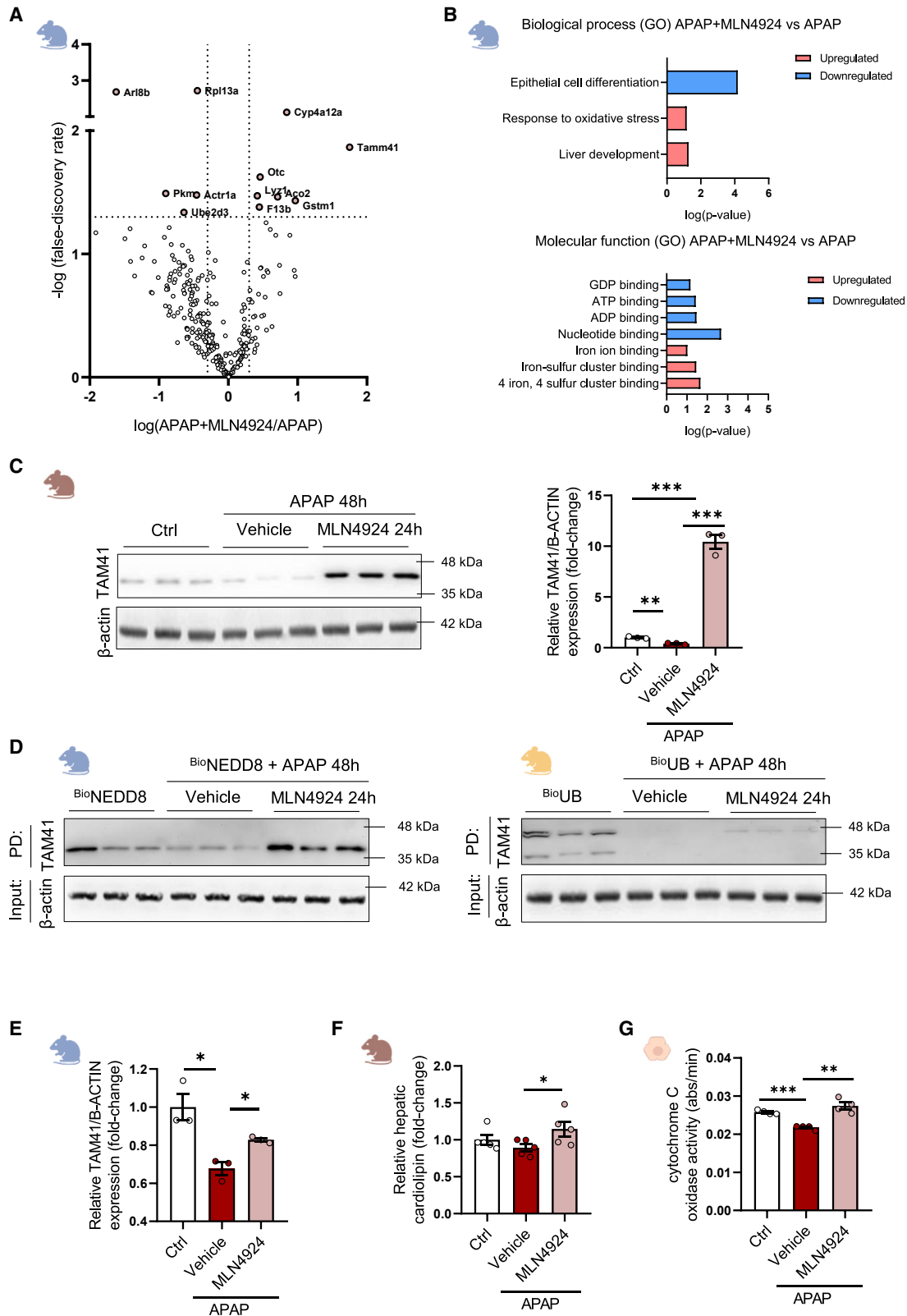
(B) Liver necrosis areas over the total area in percentage was assessed by H&E staining and a total of 5 pictures per animal were evaluated in a total of 5 mice per group ($n = 5$). Scale bar corresponds to 200 μ m.

(C) Cell death was determined by TUNEL assay liver tissue ($n = 5$). Scale bar corresponds to 100 μ m.

(D) Inflammation was assessed by F4/80 staining ($n = 5$). Scale bar corresponds to 200 μ m.

(E) Tumor necrosis factor (TNF) and interleukin-6 (IL-6) levels were determined by ELISA assay in mice serum after 48 h of APAP overdose ($n = 5$ per group).

(F) Transaminase ALT and AST levels were measured in mice serum after 48 h of APAP overdose ($n = 5$ per group). Data are shown as mean \pm SEM. * $p < 0.05$, ** $p < 0.01$, *** $p < 0.001$ and **** $p < 0.0001$ are shown (Student’s test).



(legend on next page)

APAP-induced hepatocyte damage through enhanced mitochondrial function and diminished ROS generation.

In line with these findings, genes related with mitochondrial fusion and fission biogenesis as well as mitophagy²⁹ were significantly downregulated under APAP treatment in WT primary hepatocytes, while blocking neddylation seemed to avoid this tendency (Figure 4B).

NAPQI emerges as a particularly deleterious byproduct resulting from the catabolism of APAP.³⁰ Its formation instigates GSH depletion, leading to mitochondrial dysfunction and necrosis, consequently intensifying the inflammatory response within the hepatic tissue.¹⁷ Importantly, in the context of mice under MLN4924 treatment during APAP overdose, there was an increase in the ratio of reduced GSH to oxidized GSH (GSH/GSSG), as shown in Figure 4C. Accordingly, heme oxygenase 1 and nitric oxide synthase 2 expression was also altered because of redox cellular regulation under neddylation inhibition (Figure 4D).

Overall, these results underline the significance of neddylation disruptions in mitochondrial activity in DILI and how blocking this PTM restores hepatocyte survival by reducing ROS and reestablishing energetic metabolism.

Tam41 modulates the beneficial effects of MLN4924 treatment in primary hepatocytes exposed to APAP overdose

To gain insight into the functional consequences of increased TAM41 levels due to PTM, we incubated primary hepatocytes in a medium with and without APAP for 6 h in the presence and absence of MLN4924 treatment and *Tam41* silencing (Figure S4A). Blocking neddylation abrogates APAP cell death; in contrast, *Tam41* inhibition reversed the beneficial effect, with concomitant increase in the TUNEL assay (Figures 5A and S4B). These data are further sustained by lower mitochondrial activity and greater ROS production, assessed by MitoTracker and MitoSOX respectively, in the lack of *Tam41* (Figures 5A and S4B). Under these circumstances, the absence of *Tam41* abolished the induction of mitochondrial membrane potential resulting from MLN4924 treatment (Figure 5B), according to a reduction in cardiolipin levels (Figure 5C).

These findings align with the observed increases in extracellular ATP levels in APAP-treated hepatocytes and in the absence

of *Tam41* but in the presence of MLN4924, serving as an indicator of the apoptotic response. Conversely, intracellular ATP levels were significantly reduced in APAP-treated cells, and this effect was reversed upon blocking neddylation. Silencing of *Tam41* abolished the restoration of ATP levels. (Figure 5D). Taken together, these results suggest that the absence of neddylation confers protection against liver damage induced by APAP overdose, mediated in part by *Tam41*.

Overdoses of APAP have been demonstrated to disrupt the activities of complex I and complex II in rat hepatocytes both *in vitro* and *in vivo*, leading to heightened oxidative stress and reduced ATP production.^{30,31} In this context, we investigated the activity of complex I in the presence or absence of MLN4924 and modulation of *Tam41* expression. It was observed that blocking neddylation restored the activity of complex I, which was impaired during APAP overdose (Figure 5E), whereas silencing of *Tam41* reversed this effect.

Based on these findings and recognizing the critical dependence of complex I activity on the NAD/NADH ratio, both molecules were evaluated under the same experimental conditions described earlier.³² The results revealed an increase in NAD levels and a reduction in NADH levels, leading to a higher NAD/NADH ratio when neddylation was blocked, thereby mitigating the effects of APAP. Conversely, the absence of *Tam41* once again hindered these regulatory effects (Figure 5F).

To gain deeper insights into the mechanism behind APAP injury, we utilized Tamm41 (GenBank: NM_026894) Mouse Tagged ORF Clone (OriGene) to induce *Tam41* overexpression in primary hepatocytes (Figure S4C). The results prominently demonstrate the protective effect conferred by increased levels of *Tam41* during APAP overdose (Figures 5G and S4D).

These observations underscore the significance of neddylation in mitochondrial function, with *Tam41* playing a key mediating role.

TAM41 shows a critical role in the protective mechanisms of neddylation inhibition against AILI

The role of TAM41 was assessed in preclinical animal models exposed to APAP-induced toxicity. Following an APAP overdose, mice received a single dose of MLN4924 24 h later. Twelve hours post-MLN4924 treatment, *Tam41* was silenced in the mice. The

Figure 3. Proteomic characterization of neddylated proteins in transgenic ^{Bio}NEDD8 mice treated with 360 mg/kg of APAP overdose and 24 h later administered MLN4924 treatment

(A) Volcano plot representation of specific proteins regulated in ^{Bio}NEDD8 mice treated with APAP overdose and 24 h later with 60 mg/kg MLN4924 ($n = 4$) in comparison with APAP overdose mice group ($n = 3$) after 24 h of APAP overdose.

(B) Gene Ontology (GO) biological processes and GO molecular functions upregulated and downregulated in ^{Bio}NEDD8 mice treated with APAP overdose and 24 h later with MLN4924 ($n = 4$) in comparison with APAP overdose mice group ($n = 3$).

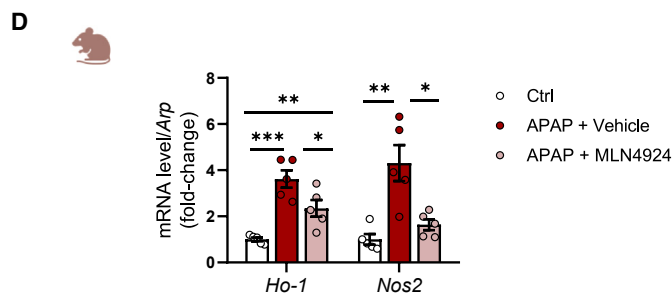
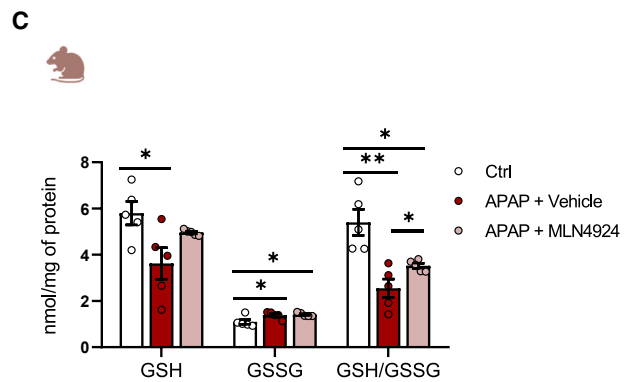
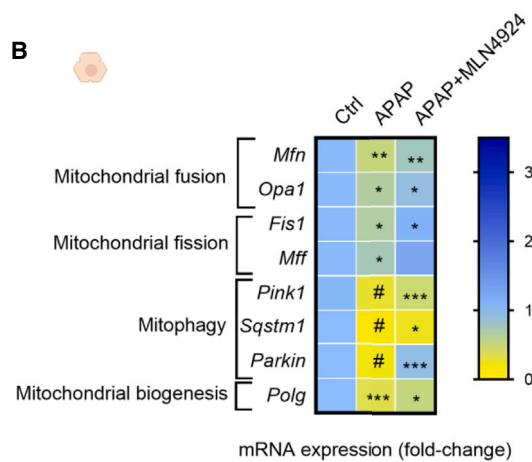
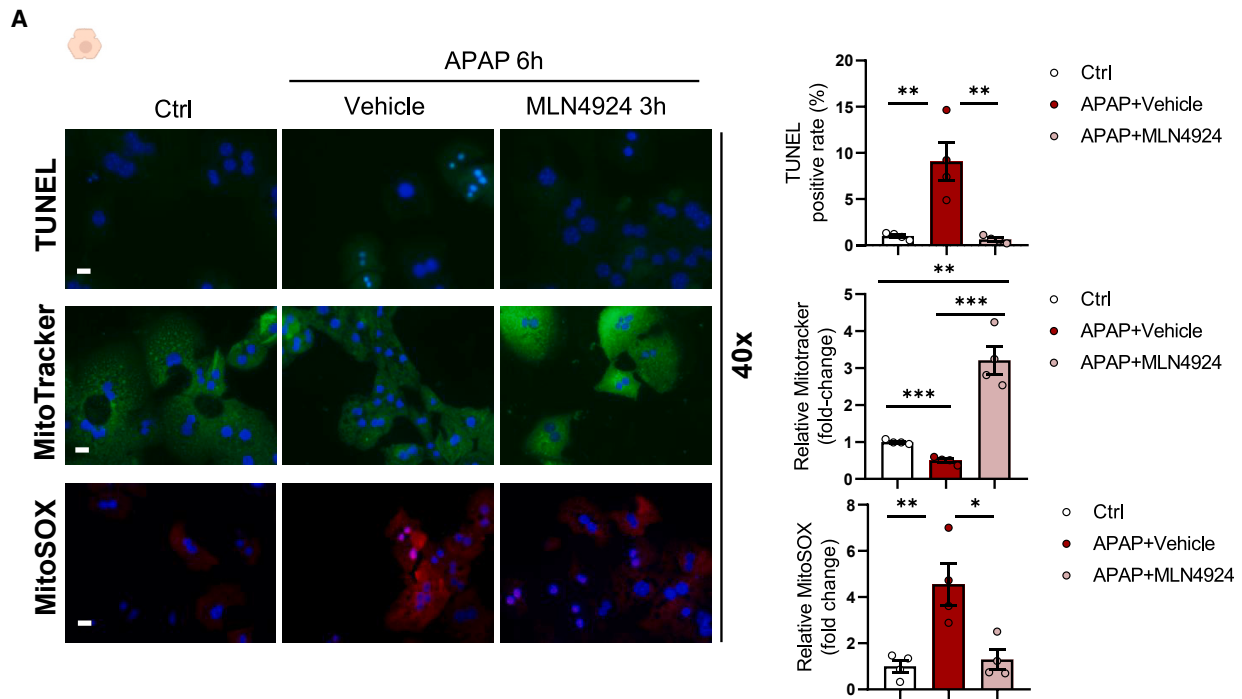
(C) Protein expression levels of TAM41 in total liver homogenate of WT mice ($n = 3$), treated with APAP overdose and 24 h later with MLN4924 ($n = 3$) compared with a control group ($n = 3$). β -Actin was used as a loading control.

(D) Protein expression levels of TAM41 after pull-down enrichment of biotinylated proteins in ^{Bio}NEDD8 mice treated with APAP overdose ($n = 3$) and 24 h later with MLN4924 ($n = 3$) compared with a control group ($n = 3$). β -Actin was used as a loading control from the input protein extract. Protein expression levels of TAM41 after pull-down enrichment of biotinylated proteins in ^{Bio}UB mice treated with APAP overdose ($n = 3$) and 24 h later with MLN4924 ($n = 3$) compared with a control group ($n = 3$). β -Actin was used as a loading control from the input protein extract.

(E) Quantification of the western blot obtained from the immunoprecipitation of NEDD8 and western blot against TAM41 in WT mice treated with APAP overdose ($n = 3$) and 24 h later with MLN4924 ($n = 3$) compared with a control group ($n = 3$).

(F) Hepatic cardiolipin levels in WT mice treated with APAP overdose ($n = 5$) and 24 h later with MLN4924 ($n = 5$) compared with a control group ($n = 5$).

(G) Cytochrome c oxidase activity was determined in WT mice hepatocytes treated with APAP overdose ($n = 4$) and 24 h later with MLN4924 ($n = 4$) compared with a control group ($n = 4$). Data are shown as mean \pm SEM. * $p < 0.05$, ** $p < 0.01$ and *** $p < 0.001$ are shown (Student's test).



(legend on next page)

mice were sacrificed 48 h after the APAP overdose, and *Tam41* expression was analyzed by RNA and protein expression assessment (Figures S5A and S5B). Importantly, the liver parenchyma of these mice was characterized by H&E staining, revealing increased necrotic areas in the si*Tam41* mice group compared to the unrelated control (Figures 6A and S5C). The same results were confirmed by TUNEL assay (Figures 6A and S5C). The quantification at a higher magnification is shown at Figure S5C. Consistent with these findings, an exacerbated inflammatory response and elevated levels of ROS were observed in the livers where *Tam41* was silenced as assessed by F4/80 and dihydroethidium, respectively (Figures 6A and S5C).

Finally, as *Tam41* is involved in the cardiolipin synthesis,¹⁶ we evaluated CL levels in the presence and absence of *Tam41* under APAP overdose with or without MLN4924 treatment. We observed a significant decrease of the hepatic cardiolipin levels under silencing *Tam41* in comparison to the unrelated control, suggesting the importance of *Tam41* in the cardiolipin synthesis (Figure 6B). In this study, we examined the levels of diacylglycerides (DG) associated with cardiolipin metabolism. Notably, DG levels were significantly elevated in the APAP-induced model, whereas animals treated with MLN4924 exhibited a trend toward reduced DG levels. The silencing of *Tam41* in the APAP model with blocked neddylation significantly mitigated this effect, resulting in a statistically significant increase in DG levels (Figure 6C). These results provide evidence of regulation within the cardiolipin metabolic pathway. Further analysis of the lipid content in the liver affirmed these findings; Figure 6C illustrates a metabolic shift in lipid profiles, generally characterized by a reduction in lipid content upon MLN4924 treatment, which in turn attenuated the lipid toxicity previously observed in the APAP model.^{33,34} The silencing of *Tam41* appears to reverse this effect.

Finally, we examined the activities of complex I and II in the presence or absence of MLN4924 and the modulation of *Tam41* expression. Our findings revealed that blocking neddylation restored the activities of complex I and II, which had been impaired during APAP overdose (Figure 6D). Conversely, silencing of *Tam41* reversed this effect (Figure 6D).

These findings reflected the significance of neddylation disruption in AILI and how inhibiting this PTM in liver pathology reestablished mitochondrial activity, in this case modulating a key component of cardiolipin biosynthesis in this organelle as well as inducing a rewiring in lipid metabolism.

Neddylation inhibition induced liver regeneration in preclinical APAP model

Harnessing liver regeneration is a fundamental process for restoring liver functionality and mass in DILI.³⁵ Indeed, boosting mitochondrial activity after injury may aid in liver regeneration,

which is an energy-intensive process.²⁷ The proliferative response in the liver was evaluated 48 h after APAP toxicity, comparing non-treated with MLN4924-treated mice. Analysis of proliferating cell nuclear antigen (PCNA) in liver tissue resulted in increased levels of this marker in APAP-treated mice with MLN4924 (Figure 7A). Moreover, silencing *Tam41* reduces PCNA staining in liver sections in comparison to the unrelated control (Figure S6A).

Further investigation of upstream regulator-mediated liver regeneration after APAP injury showed that hepatocyte growth factor and epidermal growth factor, ligands for the receptors c-MET and epidermal growth factor receptor (EGFR), respectively, which are considered critical for hepatocyte proliferation,³⁶ were significantly increased when neddylation was blocked (Figure 7B). Importantly, *Tgfβ* was downregulated in these experimental conditions, avoiding the negative influence that this factor has on the regenerative response in acute liver injury³⁷ (Figure 7B). Finally, changes in the activation of phospho c-MET, phospho EGFR, EGFR, cyclin D1, and PCNA were observed at this time point when neddylation was blocked (Figures 7C and S6B). Thus, targeting neddylation in the late stages of APAP toxicity can induce a regenerative response in the liver, counteracting the damage caused by the drug.

To further elucidate the regenerative response, an animal model with compromised liver regeneration was employed, involving a 600 mg/kg APAP overdose.³⁸ Intriguingly, livers from animals with inhibited neddylation exhibited a trend toward reduced necrotic areas, coupled with a significant decrease in TUNEL assay markers (Figures 7D and S7A), suggesting attenuated apoptosis. This was paralleled by a downward trend in transaminase levels (Figure S7B). Notably, these alterations were correlated with an enhanced regenerative response, as evidenced by elevated levels of PCNA and heightened activity of liver proliferation-associated signaling pathways, such as c-MET and EGFR (Figures 7D, 7E, and S7C).

DISCUSSION

DILI, most commonly caused by APAP, is a major cause of liver disease. In fact, overuse of APAP is the most conventional trigger of ALF in the United States. If the disease is not treated within a short time of its onset, liver transplantation is required, and in some cases, it can lead to death. Understanding the mechanisms by which APAP causes toxicity is therefore critical to overcoming liver injury with appropriate therapies.²

The PTM, known as neddylation, is induced in response to cellular stress conditions.³⁹ Our group and others have discovered that neddylated proteins are increased in preclinical models and in patients with liver injury, including fibrosis, NAFLD, and

Figure 4. Pharmacological neddylation inhibition by MLN4924 reduces cell death and increases mitochondrial function in primary hepatocytes and mice model treated with APAP overdose

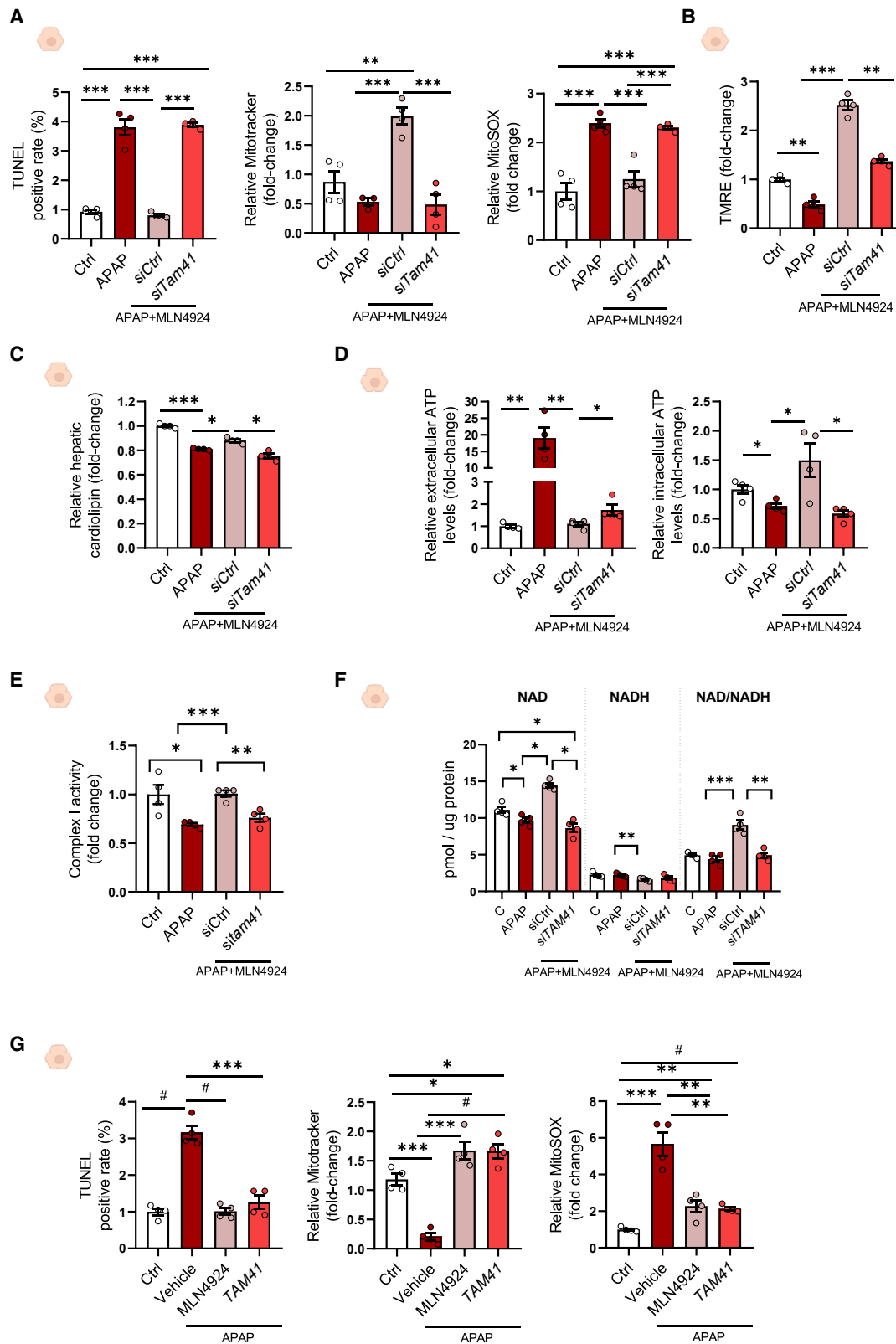
In WT hepatocytes under 10 mM APAP overdose for 6 h and treated with 3 μM MLN4924 for 3 h (*n* = 4).

(A) Cell death was evaluated by TUNEL assay, mitochondrial activity was determined by MitoTracker, and the mitochondrial ROS was determined by MitoSOX. Scale bar corresponds to 50 μm.

(B) mRNA expression levels of *Mfn1*, *Opa1*, *Fis1*, *Mff*, *Pink1*, *Sqstm1*, *Parkin*, and *Polg*.

(C) GSH, GSSG, and GSH/GSSG levels (nmol/mg of protein) were measured by liquid chromatography-mass spectrometry (HPLC-MS).

(D) mRNA expression levels of *Ho-1* and *Nos2*. Data are shown as mean ± SEM. **p* < 0.05, ***p* < 0.01, ****p* < 0.001, and #*p* < 0.00005 are shown (Student's test).



(legend on next page)

even liver cancer.^{12,14} Under these circumstances, it is critical to determine whether the increase in NEDD8-modified proteins is a compensatory mechanism for the resulting injury or part of the organ's transformation and malignancy process. Remarkable pharmacological and genetic therapeutic approaches blocking neddylation have resulted in a regression of liver injury in preclinical models.^{12,40} Thus, these data suggest that an increase in the activity of the neddylation cycle in liver disease favors the progression of the pathological condition.

The consequences of DILI due to APAP overdose include an exacerbated inflammatory response in the liver and necrotic processes due to NAPQI production, which ends in mitochondrial dysfunction.⁴¹ Neddylation has been previously described as a regulatory mechanism of mitochondrial proteins.⁴² Our results showed that an increase of neddylated proteins in the liver parenchyma of patients with AILI was associated with raised activity of this PTM pathway compared with the liver of healthy subjects. Experiments *in vitro* and preclinical mouse models with APAP overdose showed the same features even at the early stage of the disease, strongly supporting that altered neddylation promotes hepatotoxicity and adverse effects on the liver. Indeed, previous studies have indicated that a substrate of CRL3 ubiquitin ligase plays a protective role in mouse liver, providing significant defense against liver damage caused by APAP toxicity.¹⁰

Preclinical studies with MLN4924, a well-known inhibitor of NAE-1 activity, were performed to highlight the mechanism behind the overrepresentation of neddylation in DILI caused by APAP overdose. A single dose of MLN4924 was administered to the animals at 6 and 24 h after they had received an overdose of APAP. Importantly, restoring neddylation levels resulted in a halt in the DILI-associated liver pathology, consistent with a diminished necrotic area, inflammatory processes, and alanine aminotransferase (ALT) and aspartate aminotransferase (AST) levels.

Neddylation has recently been shown to play a role in controlling the shape, transport, and functionality of mitochondria.⁶ The effect of neddylation in mitochondrial function appears to vary on the cell type. For instance, MLN4924 causes oxidative stress in a variety of cancerous cells,¹¹ but it prevents an inflammatory response in liver fibrosis.⁴³ Indeed, it has no effect on healthy hepatocytes and lowers basal phosphorylation in pro-tumoral ones.¹³ Within the cell, many cullin-dependent processes have been proposed to have a role in the neddylation of mitochondrial proteins.¹¹ Considering mitochondrial impairment is one of the critical factors in DILI, a mechanistic explanation of how neddylation modifies mitochondrial proteins will advance our knowledge of mitochondrial physiological and pathophysiological functions. To do this, we have employed a whole-body^{bio}NEDD8

and^{bio}UB transgenic AILI preclinical animal model.⁴⁴ These mice allow us to characterize the landscape of the neddylated and ubiquitinated liver proteome *in vivo*, in both a healthy state and under APAP toxicity, as well as the effects of blocking neddylation by MLN4924 treatment. Under these circumstances, we have identified increased levels of mitochondrial protein TAM41 involved in the cardiolipin synthesis in the^{bio}NEDD8 and^{bio}UB mice under APAP overdose in the presence of MLN4924 validated by immunoprecipitation of NEDD8 and western blot against TAM41. These results are compatible with a regulation of neddylated TAM41 by the CRLs under DILI conditions with its consequent degradation by the ubiquitin proteome system blocked under the effect of neddylation inhibition. The findings were corroborated using primary hepatocytes where the inhibition of protein synthesis by cycloheximide was employed, resulting in a marked increase in protein stability. Notably, the co-treatment with MG132 and MLN4924, alongside cycloheximide, was observed to elevate the levels of TAM41 in the early stages of the experiment. Accordingly with these results, cullin neddylation is necessary for CRL activation,⁴⁵ being previously demonstrated that CRLs play a crucial role in the control of mitochondrial shape, functions, and protein degradation. Therefore, these data pointed out the identification of a new targeted mitochondrial protein neddylated and implicated in DILI pathology.

Phospholipids are the major components of cellular membranes located in the mitochondria.⁴⁶ Phosphatidic acid is converted to CDP-DAG by CDP-DAG synthase⁴⁷ and then branched into several pathways, one of which leads to the synthesis of cardiolipin, where TAM41 is involved. CL is a mitochondria-specific phospholipid required for proper mitochondrial function.⁴⁸ We have identified that CL is significantly upregulated in the livers of mice given an APAP overdose in the presence of MLN4924 versus those where only APAP was provided. Additionally, a significant rewiring of lipid content was identified, blocking neddylation versus the lipotoxicity observed in the animals treated with APAP alone. These results are consistent with an increase in TAM41 levels under these experimental conditions. Cardiolipin is important in several processes, including oxidative phosphorylation.⁴⁹ Consequently, we have shown that inhibiting neddylation in the context of an APAP overdose recovers the activities of hepatic mitochondrial complexes I and II. This correlates with a rise in mitochondrial membrane potential, augmented ATP synthesis, and a diminished production of mitochondrial ROS.

These data suggest that preventing TAM41 degradation by blocking neddylation restores mitochondrial activity in AILI and halts liver injury.

Finally, previous reports have shown that the energy status of hepatocytes affects liver regeneration.²⁸ In this regard,

Figure 5. Tam41 silencing in primary hepatocytes abolishes the beneficial effect of MLN4924 treatment and recovering TAM41 levels by overexpression resembled MLN4924 treatment

(A) Cell death was evaluated by TUNEL assay, mitochondrial activity was determined by MitoTracker, and the mitochondrial ROS was determined by MitoSOX. (B–F) Mitochondrial potential membrane, (C) hepatic cardiolipin, (D) extracellular and intracellular ATP levels, (E) complex I mitochondrial activity, and (F) NADH and NAD⁺ levels (pmol/mg of protein) in WT hepatocytes under 10 mM APAP overdose for 6 h and treated with 3 μM MLN4924 + siTam41 (n = 4). (G) Cell death was evaluated by TUNEL assay, mitochondrial activity was determined by MitoTracker, and the mitochondrial ROS was determined by MitoSOX in WT hepatocytes under 10 mM APAP overdose for 6 h and treated with 3 μM MLN4924 + overexpression of Tam41 (n = 4). Data are shown as mean ± SEM. *p < 0.05, **p < 0.01, ***p < 0.001, and #p < 0.00005 are shown (Student's test).

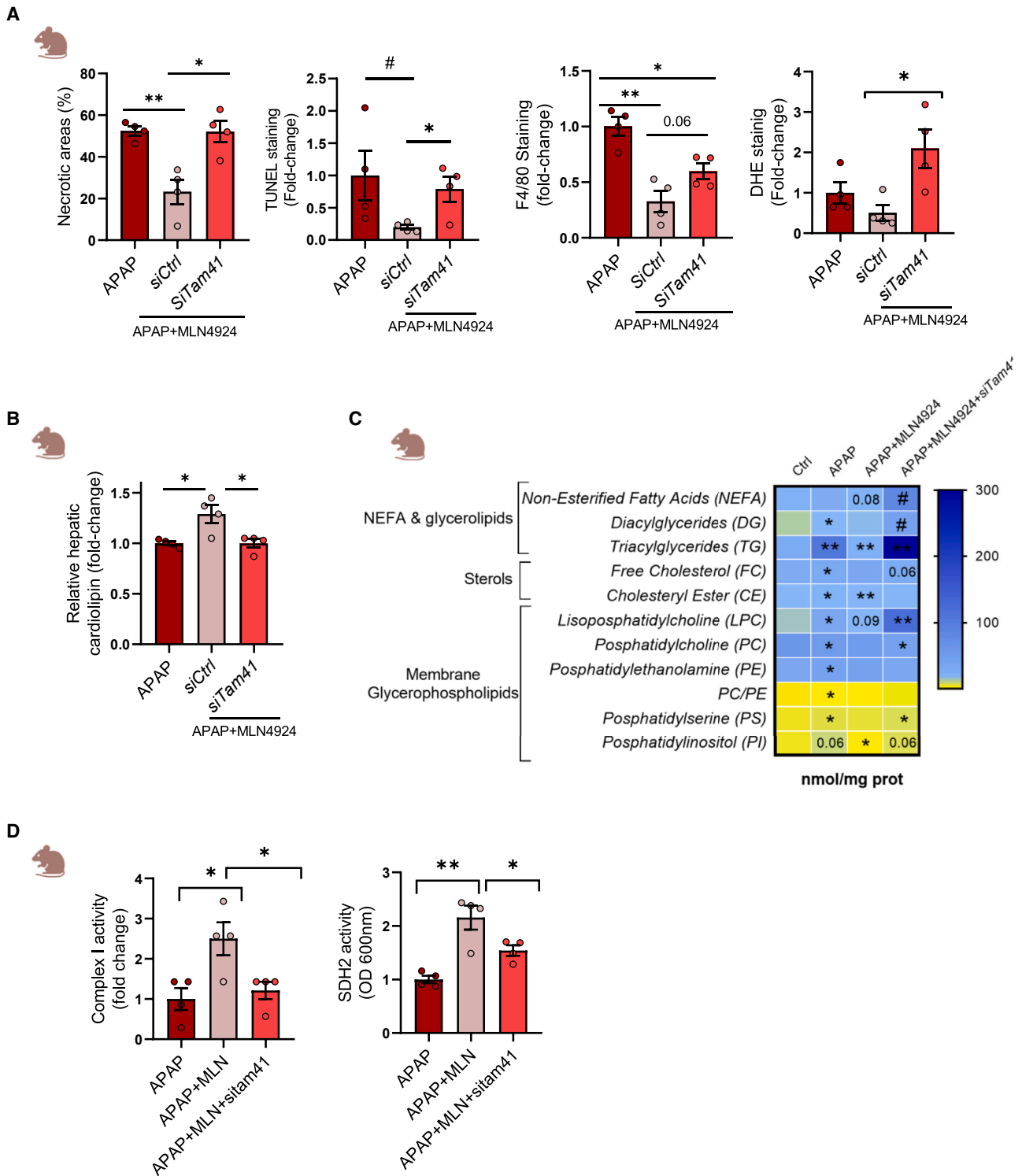


Figure 6. Tam41 silencing in mice suppresses the positive effect of MLN4924 treatment

In the preclinical mice model, mice were treated with a toxic dose of APAP ($n = 4$), and 24 h later these mice received MLN4924 in a single dose ($n = 4$). Twelve hours before MLN4924 treatment, mice were silenced Tam41 ($n = 4$). Mice were sacrificed 48 h after APAP overdose.

(A) Liver necrosis was assessed by H&E staining. Cell death was evaluated by TUNEL. Inflammation was assessed by F4/80 staining. Oxidative stress was evaluated by dihydroethidium (DHE).

(B) Hepatic cardiolipin quantification.

(legend continued on next page)

increasing mitochondrial activity without increasing collateral ROS production during MLN4924 treatment of DILI caused by APAP overdose even at 600 mg/kg, where liver regeneration was compromised,³⁸ induced a hepatic regenerative response that aids in restoring AILI.

In conclusion, neddylation is overrepresented in AILI in patients and preclinical animal models and impairs mitochondrial activity through PTM of TAM41 among other proteins, modulating cardiolipin levels. Pharmacological intervention by MLN4924 ameliorates liver injury by maintaining mitochondrial functionality and promoting the regeneration process.

Limitations of the study

Our research has unveiled a connection between neddylation dynamics and the pathogenesis AILI, with the intervention of MLN4924—NAE-1—displaying protective attributes. However, it is crucial to recognize several constraints inherent to this study. A crucial aspect that remains elusive is the identification of specific neddylation or ubiquitination sites on TAM41. Determining these sites is essential to understand the regulatory mechanisms of TAM41 and its consequential effects on hepatocyte viability. Moreover, the challenge of extrapolating results from our animal models to human AILI cannot be overstated, given the intricate nature of DILI in humans, which is a mosaic influenced by a broad spectrum of genetic and environmental factors. There is also an imperative need for meticulous determination of the therapeutic window for MLN4924 treatment in AILI, which involves optimizing the timing and dosing to ensure therapeutic efficacy while mitigating potential adverse effects.

STAR★METHODS

Detailed methods are provided in the online version of this paper and include the following:

- **KEY RESOURCES TABLE**
- **RESOURCE AVAILABILITY**
 - Lead contact
 - Materials availability
 - Data and code availability
- **EXPERIMENTAL MODEL AND STUDY PARTICIPANT DETAILS**
 - Human samples and clinical information
 - Preclinical studies and animal maintenance
 - ^{Bio}NEDD8 and ^{Bio}UBIQUITIN (^{Bio}UB) transgenic mice model
 - Preclinical model of acetaminophen overdose and treatments
 - Isolation and culture of primary hepatocytes
- **METHOD DETAILS**
 - Hepatocytes transfections and drug treatments
 - NEDD8 ELISA assay
 - Interleukin 6 (IL-6) ELISA assay
 - Tumor necrosis factor (TNF) ELISA assay
 - Cardiolipin assay quantification
 - Transaminases quantification in serum
 - Histological procedures
 - Hematoxylin and eosin (H&E)

- TUNEL assay for cell death detection *in vitro* cells
- TUNEL assay for cell death detection in tissue
- Dihydroethidium (DHE) staining
- Streptavidin pull-down assay
- Protein immunoprecipitation (IP)
- Proteomics analysis by LC-MS/MS
- Metabolomics analysis
- Lipid quantification
- RNA isolation and quantitative Real-Time PCR (RT-PCR)
- Protein isolation and western blotting
- Determination of mitochondrial reactive oxygen species (ROS)
- Mitochondrial labeling
- ATP determination
- Cytochrome *c* oxidase activity measurement in mitochondrial membranes
- Determination of the mitochondrial membrane potential
- Succinate dehydrogenase assay kit
- Complex I Enzyme activity assay kit
- NAD⁺/NADH Assay Kit

● QUANTIFICATION AND STATISTICAL ANALYSIS

SUPPLEMENTAL INFORMATION

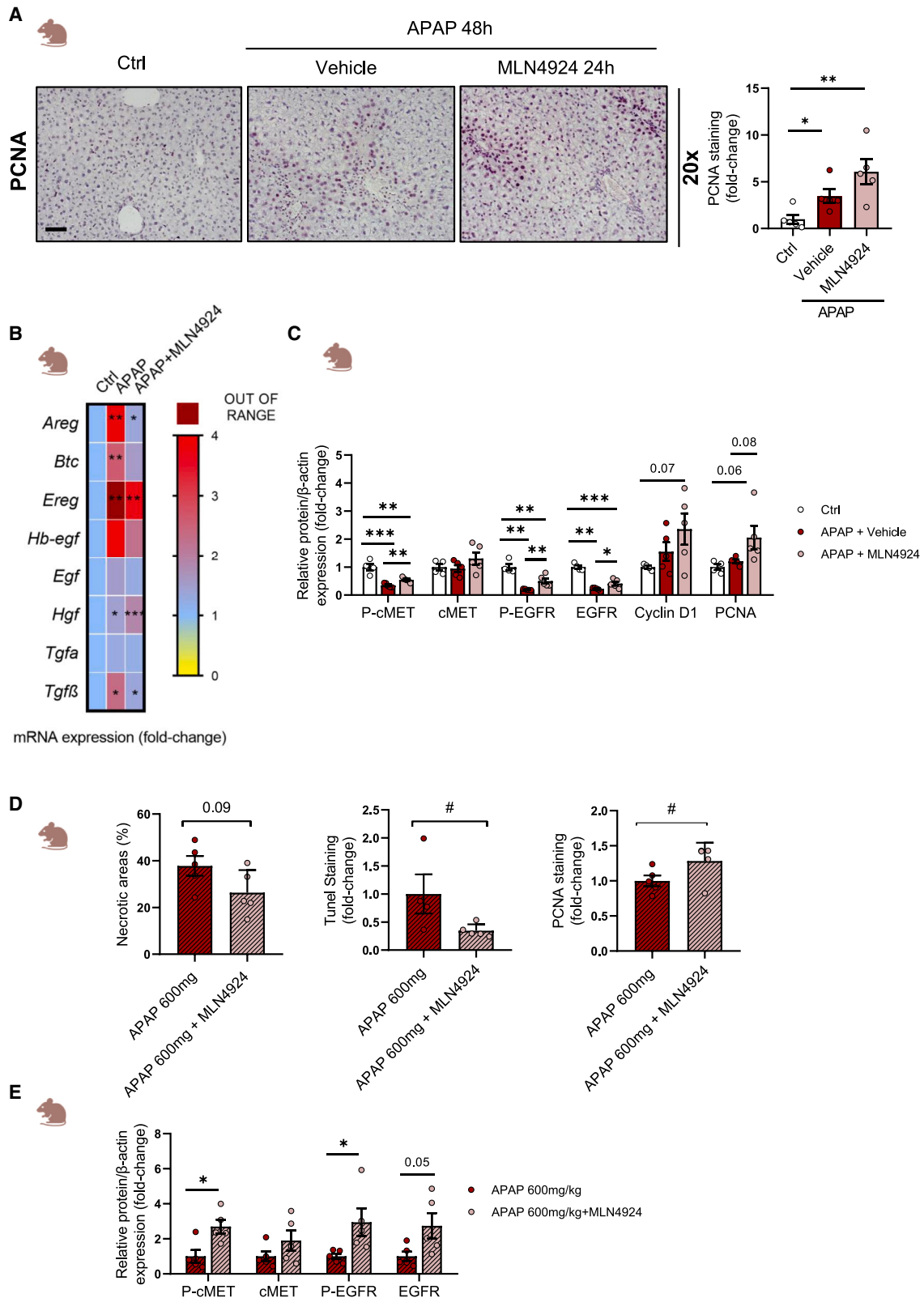
Supplemental information can be found online at <https://doi.org/10.1016/j.xcrm.2024.101653>.

ACKNOWLEDGMENTS

This work was supported by grants from Ministerio de Ciencia, Innovación y Universidades MICINN: PID2020-117116RB-I00 CEX2021-001136-S integrado en el Plan Estatal de Investigación Científica y Técnica e Innovación, cofinanciado con Fondos FEDER (for M.L.M.-C.); Ministerio de Ciencia e Innovación, Programa Retos-Colaboración RTC2019-007125-1 (for M.L.M.-C.); Instituto de Salud Carlos III, Proyectos Investigación en Salud DTS20/00138 (for M.L.M.-C.); La Caixa Scientific Foundation (HR17-00601) (for M.L.M.-C.); La Caixa Consortium (for M.L.M.-C.); Ayudas Fundación Científica AECC para proyectos coordinados (IGTP-AECC_2022-042) (for M.L.M.-C.); Transferencia tecnológica 2022 (6/12/TT/2022/00001) (for M.L.M.-C.); Desarrollo Tecnológico en Salud (DTS20/00138) (for M.L.M.-C.); Ayudas a proyectos de investigación y desarrollo en salud (2023333041) (for M.L.M.-C.); Health Research 2017 (HR17-00601) (for M.L.M.-C.); Caixa Impulse Innovation 2023 (CI23-20155) (for M.L.M.-C.); PhD fellowship from AECC (PRDVZ172010SERR) awarded to M.S.-M.; FEDER/Ministerio de Ciencia, Innovación y Universidades-Agencia Estatal de Investigación PID2021-126096NB-I00 and RED2018-102379-T; and Xunta de Galicia 2021-CP085 and 2020-PG0157 to R.N. This work was supported by a PhD fellowship from MINECO (REF BES-2017-080435) awarded to I.G.-R., PRE2019-088771 awarded to C.G.-P.; C.M.R.-G. was supported by a postdoctoral contract Margarita Salas (University of Extremadura) from the Program of Requalification of the Spanish University System (Spanish Ministry of Universities) financed by the European Union – NextGenerationEU; PRE2018-084840 awarded to M.M.-G.; PRE2021-097073 awarded to P.P.-S., by Spanish Ministerio de Ciencia e Innovación (MICINN); PRDVZ233980ZAPA awarded to L.E.Z.-P. by Ayudas Predoctorales AECC Bizkaia 2023; grants BFU2010-17857 and PID2019-109055RB-I00, Spanish Ministry of Economy and Competitiveness grants BFU2013-47531-R and BFU2016-77408-R, and also by ERA-Net E-Rare EJP RD Joint Translational Call for Rare Diseases FIGHT-CNNM2 (EJPRD19-040), and from Instituto Carlos III, Spain (REF G95229142) to L.A.M.-C.; MCIN/AEI/10.13039/501100011033 (PID2021-124425OB-I00 to P.A.) co-financed by the European Regional Development

(C) Liver quantification of lipids that belong to non-esterified fatty acids, glycerolipids, sterols, and membrane glycerophospholipids groups (nmol/mg protein). The statistical significance in the APAP column corresponds to Ctrl vs. APAP comparison, in the APAP+MLN4924 column, APAP vs. APAP+MLN4924, and in the APAP+MLN4924+siTam41 column, APAP+MLN4924 vs. APAP+MLN4924+siTam41, respectively.

(D) Complex I and complex II (succinate dehydrogenase) mitochondrial activity assay. Data are shown as mean ± SEM. **p* < 0.05, ***p* < 0.01, ****p* < 0.001, and #*p* < 0.00005 are shown (Student's test).



(legend on next page)

Fund (ERDF); and Grupos consolidados Gobierno Vasco IT1476-22 to P.A. We would like to acknowledge Begoña Rodríguez Iruretagoyena for her technical support.

AUTHOR CONTRIBUTIONS

Conceptualization, C.G.-P., M.S.-M., I.G.-R., and M.L.M.-C.; funding acquisition, L.A.M.-C. and M.L.M.-C.; experiments, C.G.-P., M.S.-M., J.S., L.M., C.C., C.M.R.-G., L.E.Z.-P., P.P.-S., M.E., R.R.-A., S.L.-O., M.M.-G., T.C.D., M.P., I.A., D.X., P.A., F.E., L.A.M.-C., R.N., P.I., J.C., S.M., M.V.M., H.L.R., R.J.A., M.I.L., N.G.-U., U.M., and I.G.-R.; supervision, I.G.-R. and M.L.M.-C.; writing – original draft and review and editing, C.G.-P., M.S.-M., I.G.-R., and M.L.M.-C. All authors have revised and approved the final version of the manuscript.

DECLARATION OF INTERESTS

The authors declare no competing interests.

Received: September 27, 2023

Revised: February 28, 2024

Accepted: June 19, 2024

Published: July 16, 2024

REFERENCES

- Suk, K.T., and Kim, D.J. (2012). Drug-induced liver injury: present and future. *Clin. Mol. Hepatol.* **18**, 249–257. <https://doi.org/10.3350/cmh.2012.18.3.249>.
- Lee, W.M. (2020). Acetaminophen Toxicity: A History of Serendipity and Unintended Consequences. *Clin. Liver Dis.* **16**, 34–44. <https://doi.org/10.1002/clid.984>.
- Lee, W.M. (2017). Acetaminophen (APAP) hepatotoxicity—Isn't it time for APAP to go away? *J. Hepatol.* **67**, 1324–1331. <https://doi.org/10.1016/j.jhep.2017.07.005>.
- Licata, A., Minissale, M.G., Stankevičiūtė, S., Sanabria-Cabrera, J., Lucena, M.I., Andrade, R.J., and Almasio, P.L. (2022). N-Acetylcysteine for Preventing Acetaminophen-Induced Liver Injury: A Comprehensive Review. *Front. Pharmacol.* **13**, 828565. <https://doi.org/10.3389/fphar.2022.828565>.
- Yan, M., Huo, Y., Yin, S., and Hu, H. (2018). Mechanisms of acetaminophen-induced liver injury and its implications for therapeutic interventions. *Redox Biol.* **17**, 274–283. <https://doi.org/10.1016/j.redox.2018.04.019>.
- Zhou, Q., Zheng, Y., and Sun, Y. (2021). Neddylation regulation of mitochondrial structure and functions. *Cell Biosci.* **11**, 55. <https://doi.org/10.1186/s13578-021-00569-6>.
- Chung, D., and Dellaire, G. (2015). The role of the COP9 signalosome and neddylation in DNA damage signaling and repair. *Biomolecules* **5**, 2388–2416.
- Enchev, R.I., Schulman, B.A., and Peter, M. (2015). Protein neddylation: Beyond cullin-RING ligases. *Nat. Rev. Mol. Cell Biol.* **16**, 30–44. <https://doi.org/10.1038/nrm3919>.
- Soucy, T.A., Dick, L.R., Smith, P.G., Milhollen, M.A., and Brownell, J.E. (2010). The NEDD8 conjugation pathway and its relevance in cancer biology and therapy. *Genes Cancer* **1**, 708–716.
- Zhou, H., Lu, J., Chinnaswamy, K., Stuckey, J.A., Liu, L., McEachern, D., Yang, C.Y., Bernard, D., Shen, H., Rui, L., et al. (2021). Selective inhibition of cullin 3 neddylation through covalent targeting DCN1 protects mice from acetaminophen-induced liver toxicity. *Nat. Commun.* **12**, 2621.
- Zhou, Q., Li, H., Li, Y., Tan, M., Fan, S., Cao, C., Meng, F., Zhu, L., Zhao, L., Guan, M.X., et al. (2019). Inhibiting neddylation modification alters mitochondrial morphology and reprograms energy metabolism in cancer cells. *JCI Insight* **4**, e121582.
- Serrano-Maciá, M., Simón, J., González-Rellan, M.J., Azkargorta, M., Goikoetxea-Usandizaga, N., Lopitz-Otsoa, F., De Urturi, D.S., Rodríguez-Agudo, R., Lachiondo-Ortega, S., Mercado-Gomez, M., et al. (2021). Neddylation inhibition ameliorates steatosis in NAFLD by boosting hepatic fatty acid oxidation via the DEPTOR-mTOR axis. *Mol Metab* **53**, 101275.
- Barbier-Torres, L., Delgado, T.C., García-Rodríguez, J.L., Zubieta-Franco, I., Fernández-Ramos, D., Buqué, X., Cano, A., Gutiérrez-de Juan, V., Fernández-Domínguez, I., Lopitz-Otsoa, F., et al. (2015). Stabilization of LKB1 and Akt by Neddylation Regulates Energy Metabolism in Liver Cancer. *Oncotarget* **6**, 2509–2523. www.impactjournals.com/oncotarget/.
- Delgado, T.C., Barbier-Torres, L., Zubieta-Franco, I., Lopitz-Otsoa, F., Varela-Rey, M., Fernández-Ramos, D., and Martínez-Chantar, M.L. (2018). Neddylation, a novel paradigm in liver cancer. *Transl. Gastroenterol. Hepatol.* **3**, 37. <https://doi.org/10.21037/tgh.2018.06.05>.
- Olaizola, P., Lee-Law, P.Y., Fernandez-Barrena, M.G., Alvarez, L., Cadamuro, M., Azkargorta, M., O'Rourke, C.J., Caballero-Camino, F.J., Olaizola, I., Macias, R.I.R., et al. (2022). Targeting NAE1-mediated protein hyper-NEDDylation halts cholangiocarcinogenesis and impacts on tumor-stroma crosstalk in experimental models. *J. Hepatol.* **77**, 177–190.
- Tamura, Y., Harada, Y., Nishikawa, S.I., Yamano, K., Kamiya, M., Shiota, T., Kuroda, T., Kuge, O., Sesaki, H., Imai, K., et al. (2013). Tam41 is a CDP-diacylglycerol synthase required for cardiolipin biosynthesis in mitochondria. *Cell Metab.* **17**, 709–718.
- Villanueva-Paz, M., Morán, L., López-Alcántara, N., Freixo, C., Andrade, R.J., Lucena, M.I., and Cubero, F.J. (2021). Oxidative stress in drug-induced liver injury (DILI): From mechanisms to biomarkers for use in clinical practice. *Antioxidants* **10**, 390–435. <https://doi.org/10.3390/antiox10030390>.
- Zubieta-Franco, I., Fernández-Tussy, P., Barbier-Torres, L., Simon, J., Fernández-Ramos, D., Lopitz-Otsoa, F., Gutiérrez-de Juan, V., de Davallillo, S.L., Duce, A.M., Iruzebieta, P., et al. (2017). Deregulated neddylation in liver fibrosis. *Hepatology* **65**, 694–709.
- Ju, C., and Reilly, T. (2012). Role of immune reactions in drug-induced liver injury (DILI). *Drug Metab. Rev.* **44**, 107–115. <https://doi.org/10.3109/03602532.2011.645579>.

Figure 7. Pharmacological neddylation inhibition improves mitochondrial function and regenerative response in preclinical mice model treated with an APAP overdose and 24 h later with MLN4924 treatment

In the preclinical mice model under APAP-induced toxicity of 360 mg/kg ($n = 5$), 24 h after APAP administration, mice received MLN4924 in a single dose ($n = 5$). Mice were sacrificed 48 h after APAP overdose.

(A) PCNA expression by immunohistochemistry ($n = 5$). Scale bar corresponds to 100 μm .

(B) mRNA expression levels of *Areg*, *Btc*, *Ereg*, *Hb-egf*, *Egf*, *Hgf*, *Tgfa*, and *Tgfb* ($n = 4$).

(C) Protein expression levels of P-cMET, cMET, p-EGFR, EGFR, cyclin D1, and PCNA. β -Actin was used as a loading control ($n = 5$). In the preclinical mice model under APAP-induced toxicity of 600 mg/kg ($n = 5$), 6 h after APAP administration, mice received MLN4924 in a single dose ($n = 5$). Mice were sacrificed 24 h after APAP overdose.

(D) Liver necrosis was assessed by H&E staining. Cell death was evaluated by TUNEL. Regeneration was evaluated by PCNA staining. Scale bar corresponds to 200 μm .

(E) Quantification of protein expression levels of P-cMET, cMET, p-EGFR, and EGFR. β -Actin was used as a loading control ($n = 5$). Data are shown as mean \pm SEM. * $p < 0.05$, ** $p < 0.01$, *** $p < 0.001$, and # $p < 0.00005$ are shown (Student's test).

20. Lachiondo-Ortega, S., Delgado, T.C., Baños-Jaime, B., Velázquez-Cruz, A., Díaz-Moreno, I., and Martínez-Chantar, M.L. (2022). Hu Antigen R (HuR) Protein Structure, Function and Regulation in Hepatobiliary Tumors. *Cancers* **14**, 2666. <https://doi.org/10.3390/cancers14112666>.
21. Kim, Y., Park, J.B., Fukuda, J., Watanabe, M., and Chun, Y.S. (2021). The effect of neddylation blockade on slug-dependent cancer cell migration is regulated by p53 mutation status. *Cancers* **13**, 531–621.
22. Abidi, N., and Xirodimas, D.P. (2015). Regulation of cancer-related pathways by protein NEDDylation and strategies for the use of NEDD8 inhibitors in the clinic. *Endocr. Relat. Cancer* **22**, T55–T70. <https://doi.org/10.1530/ERC-14-0315>.
23. Patil, V.A., Fox, J.L., Gohil, V.M., Winge, D.R., and Greenberg, M.L. (2013). Loss of cardiolipin leads to perturbation of mitochondrial and cellular iron homeostasis. *J. Biol. Chem.* **288**, 1696–1705.
24. Mercado-gómez, M. (2020). Multi-omics integration highlights the role of ubiquitination in ccl4-induced liver fibrosis. *Int. J. Mol. Sci.* **21**, 1–19.
25. Watson, S.A., and McStay, G.P. (2020). Functions of cytochrome c oxidase assembly factors. *Int. J. Mol. Sci.* **21**, 7254–7318. <https://doi.org/10.3390/ijms21197254>.
26. Amarez, C., Marrink, S.J., and Periole, X. (2013). Identification of cardiolipin binding sites on cytochrome c oxidase at the entrance of proton channels. *Sci. Rep.* **3**, 1263.
27. Barbier-Torres, L., Iruzubieta, P., Fernández-Ramos, D., Delgado, T.C., Taibo, D., Guitiérrez-de-Juan, V., Varela-Rey, M., Azkargorta, M., Navasa, N., Fernández-Tussy, P., et al. (2017). The mitochondrial negative regulator MCJ is a therapeutic target for acetaminophen-induced liver injury. *Nat. Commun.* **8**, 2068.
28. Goikoetxea-Usandizaga, N., Serrano-Maciá, M., Delgado, T.C., Simón, J., Fernández Ramos, D., Barriales, D., Cornide, M.E., Jiménez, M., Pérez-Redondo, M., Lachiondo-Ortega, S., et al. (2022). Mitochondrial bioenergetics boost macrophage activation, promoting liver regeneration in metabolically compromised animals. *Hepatology* **75**, 550–566.
29. Gao, Y., Chu, S., Zhang, Z., Zuo, W., Xia, C., Ai, Q., Luo, P., Cao, P., and Chen, N. (2017). Early Stage Functions of Mitochondrial Autophagy and Oxidative Stress in Acetaminophen-Induced Liver Injury. *J. Cell. Biochem.* **118**, 3130–3141.
30. Donnelly, P.J., Walker, R.M., and Racz, W.J. (1994). Inhibition of Mitochondrial Respiration in Vivo Is an Early Event in Acetaminophen-Induced Hepatotoxicity. *Arch. Toxicol.* **68**, 110–118.
31. Burcham, P.C., and Harman, A.W. (1991). Acetaminophen toxicity results in site-specific mitochondrial damage in isolated mouse hepatocytes. *J. Biol. Chem.* **266**, 5049–5054.
32. Kushnareva, Y., Murphy, A.N., and Andreyev, A. (2002). Complex I-Mediated Reactive Oxygen Species Generation : Modulation by Cytochrome c and NAD(P) T Oxidation-Reduction State. *Biochem. J.* **368**, 545–553.
33. Chen, S., Lu, Z., Jia, H., Yang, B., Liu, C., Yang, Y., Zhang, S., Wang, Z., Yang, L., Li, S., et al. (2023). Hepatocyte-specific Mas activation enhances lipophagy and fatty acid oxidation to protect against acetaminophen-induced hepatotoxicity in mice. *J. Hepatol.* **78**, 543–557.
34. Simon, J., Nuñez-García, M., Fernández-Tussy, P., Barbier-Torres, L., Fernández-Ramos, D., Gómez-Santos, B., Buqué, X., Lopitz-Otsoa, F., Goikoetxea-Usandizaga, N., Serrano-Macia, M., et al. (2020). Targeting Hepatic Glutaminase 1 Ameliorates Non-alcoholic Steatohepatitis by Restoring Very-Low-Density Lipoprotein Triglyceride Assembly. *Cell Metab.* **31**, 605–622.e10.
35. Michalopoulos, G.K. (2013). Principles of liver regeneration and growth homeostasis. *Compr. Physiol.* **3**, 485–513.
36. Bhushan, B., Gunewardena, S., Edwards, G., and Apte, U. (2020). Comparison of liver regeneration after partial hepatectomy and acetaminophen-induced acute liver failure: A global picture based on transcriptome analysis. *Food Chem. Toxicol.* **139**, 111186.
37. Fabregat, I., Moreno-Càceres, J., Sánchez, A., Dooley, S., Dewidar, B., Giannelli, G., and Ten Dijke, P.; IT-LIVER Consortium (2016). TGF- β signaling and liver disease. *FEBS J.* **283**, 2219–2232. <https://doi.org/10.1111/febs.13665>.
38. Kotulkar, M., Paine-Cabrera, D., Abernathy, S., Robarts, D.R., Parkes, W.S., Lin-Rahardja, K., Numata, S., Lebofsky, M., Jaeschke, H., and Apte, U. (2023). Role of HNF4 α -cMyc interaction in liver regeneration and recovery after acetaminophen-induced acute liver injury. *Hepatology* **78**, 1106–1117.
39. Maghames, C.M., Lobato-Gil, S., Perrin, A., Trauchessec, H., Rodriguez, M.S., Urbach, S., Marin, P., and Xirodimas, D.P. (2018). NEDDylation promotes nuclear protein aggregation and protects the Ubiquitin Proteasome System upon proteotoxic stress. *Nat. Commun.* **9**, 4376.
40. Lachiondo-Ortega, S., Mercado-Gómez, M., Serrano-Maciá, M., Lopitz-Otsoa, F., Salas-Villalobos, T.B., Varela-Rey, M., Delgado, T.C., and Martínez-Chantar, M.L. (2019). Ubiquitin-like post-translational modifications (Ubl-PTMs): Small peptides with huge impact in liver fibrosis. *Cells* **8**, 1575. <https://doi.org/10.3390/cells8121575>.
41. Yoon, E., Babar, A., Choudhary, M., Kutner, M., and Pysopoulos, N. (2016). Acetaminophen-induced hepatotoxicity: A comprehensive update. *J. Clin. Transl. Hepatol.* **4**, 131–142. <https://doi.org/10.14218/JCTH.2015.00052>.
42. Zou, T., and Zhang, J. (2021). Diverse and pivotal roles of neddylation in metabolism and immunity. *FEBS J.* **288**, 3884–3912. <https://doi.org/10.1111/febs.15584>.
43. Serrano-Maciá, M., Lachiondo-Ortega, S., Iruzubieta, P., Goikoetxea-Usandizaga, N., Bosch, A., Egia-Mendikute, L., Jiménez-Lasheras, B., Azkargorta, M., Elortza, F., Martínez-Redondo, D., et al. (2022). Neddylation tunes peripheral blood mononuclear cells immune response in COVID-19 patients. *Cell Death Discov* **8**, 316.
44. Serrano-Maciá, M., Delgado, T.C., and Martínez-Chantar, M.L. (2023). Isolation of the Hepatic Ubiquitome/NEDDylome by Streptavidin Pull-Down Assay in the Biotinylated Ubiquitin (bioUb)/Biotinylated NEDD8 (bio-NEDD8) Transgenic Mice. In *The Ubiquitin Code*, M.S. Rodríguez and R. Barrio, eds. (Springer US), pp. 151–162. https://doi.org/10.1007/978-1-0716-2859-1_11.
45. Duda, D.M., Borg, L.A., Scott, D.C., Hunt, H.W., Hammel, M., and Schulman, B.A. (2008). Structural Insights into NEDD8 Activation of Cullin-RING Ligases: Conformational Control of Conjugation. *Cell* **134**, 995–1006.
46. Schenkel, L.C., and Bakovic, M. (2014). Formation and regulation of mitochondrial membranes. *Int. J. Cell Biol.* **2014**, 709828. <https://doi.org/10.1155/2014/709828>.
47. Blunsom, N.J., and Cockcroft, S. (2020). CDP-Diacylglycerol Synthases (CDS): Gateway to Phosphatidylinositol and Cardiolipin Synthesis. *Front. Cell Dev. Biol.* **8**, 63. <https://doi.org/10.3389/fcell.2020.00063>.
48. Paradies, G., Paradies, V., Ruggiero, F.M., and Petrosillo, G. (2019). Role of cardiolipin in mitochondrial function and dynamics in health and disease: Molecular and pharmacological aspects. *Cells* **8**, 728. <https://doi.org/10.3390/cells8070728>.
49. Paradies, G., Paradies, V., Ruggiero, F.M., and Petrosillo, G. (2014). Oxidative stress, cardiolipin and mitochondrial dysfunction in nonalcoholic fatty liver disease. *World J. Gastroenterol.* **20**, 14205–14218. <https://doi.org/10.3748/wjg.v20.i39.14205>.
50. Lectez, B., Migotti, R., Lee, S.Y., Ramirez, J., Beraza, N., Mansfield, B., Sutherland, J.D., Martínez-Chantar, M.L., Dittmar, G., and Mayor, U. (2014). Ubiquitin profiling in liver using a transgenic mouse with biotinylated ubiquitin. *J. Proteome Res.* **13**, 3016–3026.
51. Barbier-Torres, L., Fortner, K.A., Iruzubieta, P., Delgado, T.C., Giddings, E., Chen, Y., Champagne, D., Fernández-Ramos, D., Mestre, D., Gomez-Santos, B., et al. (2020). Silencing hepatic MCJ attenuates non-alcoholic fatty liver disease (NAFLD) by increasing mitochondrial fatty acid oxidation. *Nat. Commun.* **11**, 3360.

52. Gonzalez-Rellan, M.J., Fernández, U., Parracho, T., Novoa, E., Fondevila, M.F., da Silva Lima, N., Ramos, L., Rodríguez, A., Serrano-Maciá, M., Perez-Mejias, G., et al. (2023). Neddylation of phosphoenolpyruvate carboxykinase 1 controls glucose metabolism. *Cell Metab.* 35, 1630–1645.e5.
53. Zubiete-Franco, I., García-Rodríguez, J.L., Lopitz-Otsoa, F., Serrano-Maciá, M., Simon, J., Fernández-Tussy, P., Barbier-Torres, L., Fernández-Ramos, D., Gutiérrez-de-Juan, V., López de Davalillo, S., et al. (2019). SUMOylation regulates LKB1 localization and its oncogenic activity in liver cancer. *EBioMedicine* 40, 406–421.
54. Li, J., Xu, Y., Long, X.D., Wang, W., Jiao, H.K., Mei, Z., Yin, Q.Q., Ma, L.N., Zhou, A.W., Wang, L.S., et al. (2014). Cbx4 governs HIF-1 α to potentiate angiogenesis of hepatocellular carcinoma by its SUMO E3 ligase activity. *Cancer Cell* 25, 547–548.
55. Tyanova, S., Temu, T., Sinitcyn, P., Carlson, A., Hein, M.Y., Geiger, T., Mann, M., and Cox, J. (2016). Perseus Platform for Proteomics Data The Perseus Computational Platform for Comprehensive Analysis of (Prote) Omics Data. *Nat. Methods* 13, 731–740.
56. Gómez-Santos, B., Saenz de Urturi, D., Nuñez-García, M., Gonzalez-Romero, F., Buque, X., Aurrekoetxea, I., Gutiérrez de Juan, V., Gonzalez-Rellan, M.J., García-Monzón, C., González-Rodríguez, Á., et al. (2020). Liver osteopontin is required to prevent the progression of age-related nonalcoholic fatty liver disease. *Aging Cell* 19.
57. Folch, J., Lees, M., and Sloane Stanley, G.H. (1957). A simple method for the isolation and purification of total lipides from animal tissues. *J. Biol. Chem.* 226, 497–509.
58. González-Recio, I., Simón, J., Goikoetxea-Usandizaga, N., Serrano-Maciá, M., Mercado-Gómez, M., Rodríguez-Agudo, R., Lachiondo-Ortega, S., Gil-Pitarch, C., Fernández-Rodríguez, C., Castellana, D., et al. (2022). Restoring cellular magnesium balance through Cyclin M4 protects against acetaminophen-induced liver damage. *Nat. Commun.* 13, 6816.
59. Rodríguez-Agudo, R., Goikoetxea-Usandizaga, N., Serrano-Maciá, M., Fernández-Tussy, P., Fernández-Ramos, D., Lachiondo-Ortega, S., González-Recio, I., Mercado-Gómez, M., Morán, L., Bizkarguenaga, M., et al. (2022). Methionine Cycle Rewiring by Targeting miR-873-5p Modulates Ammonia Metabolism to Protect the Liver from Acetaminophen. *Antioxidants* 11, 897.

STAR★METHODS

KEY RESOURCES TABLE

REAGENT or RESOURCE	SOURCE	IDENTIFIER
Antibodies		
Anti-mouse IgG, HRP-linked Antibody	Cell Signaling	Cat#t7076S; RRID: AB_3105896
Anti-rabbit IgG, HRP-linked Antibody	Cell Signaling	Cat#7074S; RRID: AB_3105897
Cyclin D1	Cell Signaling	Cat#2978; RRID: AB_2259616
Dcund1d3	Santa Cruz Biotechnology	Cat#sc-514506; RRID: AB_3105891
Egfr	Merk	Cat#06-847; RRID: AB_2096607
F4/80	Bio-Rad	Cat#MCA497BB; RRID: AB_323893
Gapdh [6C5]	Abcam	Cat#ab8245; RRID: AB_2107448
Mdm2	Proteintech	Cat#66511-1-Ig; RRID: AB_2881874
Met (c-Met) [EP1454Y] - N-terminal	Abcam	Cat#ab51067; RRID: AB_880695
Nae1	Cell Signaling	Cat#14321; RRID: AB_2798448
NEDD8 antibody for IHC	Cell Signaling	Cat#2745; RRID: AB_10695300
NEDD8 antibody IP and WB	Abcam	Cat#ab81264; RRID: AB_1640720
Pcna	Santa Cruz Biotechnology	Cat#sc-25280; RRID: AB_628109
Purified Mouse IgG1, κ Isotype Control	BD Pharmingen	Cat#557273; RRID: AB_396613
pY1068-Egfr	Cell Signaling	Cat#3777; RRID: AB_2096270
pY1230/1234/1235-cMet	MerckMillipore	Cat#07-810; RRID: AB_568851
Tam41	Abcam	Cat#ab230359; RRID: AB_3105893
Total OXPHOS Cocktail (V-ATP5A, III-UQCRC2, II-SDHB, IV-COXII, I-NDUFB8)	Abcam	Cat#ab110411; RRID: AB_2756818
Uba3	Santa Cruz Biotechnology	Cat#sc-377272; RRID: AB_3105894
β-actin	Sigma-Aldrich	Cat#A2228; RRID: AB_476697
Biological samples		
Paraffin-embedded liver AILI patients	Supplied by MD PhD Helen L Reeves	Newcastle Hospital NHS Foundation Trust (Newcastle, England)
Paraffin-embedded liver healthy transplant donors	Supplied by MD PhD Javier Crespo	Marqués de Valdecilla University Hospital (Santander, Spain)
Chemicals, peptides, and recombinant proteins		
2-hydroxypropyl-β-cyclodextrin	Sigma-Aldrich	Cat# H107-100G CAS. 128446-35-5
2-Propanol	Sigma-Aldrich	Car#I9516 CAS 67-63-0
Acetaminophen (APAP)	Sigma-Aldrich	Cat# A7085-100G CAS. 103-90-2
Acetic Acid	Sigma-Aldrich	Car# W200603 CAS 64-19-7
Acetonitrile	Sigma-Aldrich	Cat# 34851 CAS 75-05-8
Calcium chloride	Sigma-Aldrich	Cat# C5670 CAS 10043-52-4
Chloroform	Sigma-Aldrich	Cat#C2431 CAS 67-66-1
Cycloheximide	Sigma-Aldrich	C1988-1g
Collagenase type IV, CLS-4	Worthington	Cat#LS004188
Corning Collagen I, Rat Tail,	Corning	Cat#354236
Dako EnVision system, Peroxidase	Dako	Cat#K5007

(Continued on next page)

Continued

REAGENT or RESOURCE	SOURCE	IDENTIFIER
D-Glucose	Sigma-Aldrich	Cat#G7021 CAS 50-99-7
DharmaFECT 1 Transfection Reagent	Dharmacon	Cat#T-2001-01
Dihydroethidium (DHE)	Sigma	Cat#D-7008-10mg
Dimethyl pimelimidate dihydrochloride (DMP)	Sigma	Cat#80490
DL-Dithiothreitol (DTT)	Sigma-Aldrich	Cat# DTT-RO CAS 3483-12-3
DPX Mountant for histology	Sigma-Aldrich	Cat#06522
Dulbecco's Phosphate-Buffered Saline (PBS)	Gibco	Cat# 14190144
EnVision+ System HRP	Dako	Cat#K4001
Eosin B	Sigma-Aldrich	Cat#2853
Ethanol	Sigma-Aldrich	Cat#E7023 CAS 64-17-5
Fetal Bovine Serum (FBS)	GIBCO	Cat#A38401
Fluoromount g with DAPI	Southern Biotech	Cat# 0100-01
Formic Acid	PanReac AppliChem	Cat#1002641000 CAS 64-18-6
Glycol ether diamine tetraacetic acid (EGTA)	Sigma-Aldrich	Cat# E3889 CAS 67-42-5
Guanidine hydrochloride	Sigma-Aldrich	Cat#G3272 CAS 50-01-1
Harris Hematoxylin	Bio-Optica	Cat#05-06005/L
Histo-Clear I Solution	Electron Microscopy Sciences	Cat#64110-004
Hydrogen Peroxide 30% w/v	PanReac AppliChem	#Cat121076 CAS 7722-84-1
Igepal	Sigma-Aldrich	Cat#I8896 CAS 9002-93-1
Invivofectamine™ 3.0 Reagent	Invitrogen	Cat#IVFs3001
iodoacetamide (IAA)	Sigma-Aldrich	Cat#I6125 CAS 144-48-9
Isoflurane	Baxter SL	Cat#NR60378
jetPRIME	Polyplus	Cat#114-15
L-glutamine	GIBCO	Cat#25030-024
Mayer's Haematoxylin	Sigma-Aldrich	Cat# MHS16
Methanol	PanReac AppliChem	#Cat1610911714 CAS 67-56-1
MG132	Sigma-Aldrich	1211877-36-9
Minimum Essential Media	GIBCO	Cat#31095029
N-Ethylmaleimide	Sigma	Cat#23030
OCT	Pioneer	Cat#PRC/OCT
Oxygen	Air Liquide SLU	Cat#ESCG101710
Paraformaldehyde 4% solution in PBS	Santa Cruz	Cat#Sc-281692 CAS 30525-89-4
Penicillin-Streptomycin-Glutamine (100x)	GIBCO	Cat#10378016
Pevonedistat (MLN4924)	MeDChemExpress, MCE	Cat#HY-70062 CAS. 905579-51-3
Phenylmethylsulfonyl fluoride (PMSF)	Sigma-Aldrich	Cat#52332 CAS 329-98-6
Phosphatase inhibitor cocktail	Sigma-Aldrich	Cat#P2850
Ponceau S Solution	Sigma-Aldrich	Cat#P7170-1L CAS 6226-79-5
Potassium chloride	Sigma-Aldrich	Cat#G7021 CAS 7447-40-7

(Continued on next page)

Continued

REAGENT or RESOURCE	SOURCE	IDENTIFIER
Potassium ethylenediaminetetraacetate dibasic (EDTA)	Sigma-Aldrich	Cat#E9884 CAS 25102-12-9
Protease Inhibitor cocktail	Sigma-Aldrich	Cat#P8340,
Protease Inhibitor Cocktail Tablets	Roche Diagnostics	Cat#11697498001
Sodium azide	Sigma-Aldrich	Cat# S8032 CAS 26628-22-8
Sodium bicarbonate	Sigma-Aldrich	Cat#S5761 CAS 144-55-8
Sodium chloride	PanReac AppliChem	Cat#1064041000 CAS 7647-14-5
Sodium deoxycholate	Sigma-Aldrich	Cat# 30970 CAS 302-95-4
Sodium dodecyl sulfate	Sigma-Aldrich	Cat#L5750 CAS 151-21-3
Sodium fluoride	Sigma-Aldrich	Cat#S7920-100G CAS 7681-49-4
Sodium orthovanadate	Sigma-Aldrich	Cat#S6508-50G CAS 13721-39-6
Sodium phosphate dibasic	Sigma-Aldrich	Cat# 71640 CAS 7558-79-4
Sodium phosphate monobasic	Sigma-Aldrich	Cat# S0751 CAS 7558-80-7
Tris Base	Fisher	Cat#BP152-1
Triton X-100	Sigma-Aldrich	Cat# 100-500mL
Trizol	Invitrogen	Cat#15596026
Tween 20	Sigma-Aldrich	Cat# P9416
Urea	Sigma-Aldrich	Cat#U5378 CAS 57-13-6
β-mercapthoethanol	Sigma-Aldrich	Cat#M3148 CAS 60-24-2

Critical commercial assays

3,3'-Diaminobenzidine (DAB)	Sigma-Aldrich	Cat#D6815
A special microcentrifuge filter VivaClean Mini 0.8 μL m PES	Sartorius	Cat# VK01P042
ATPlite™ luminescence ATP detection kit	Perkin Elmer	Cat#6016943
Bead Ruptor Homogenizer	OMNI International	N/A
Cardiolipin Assay kit	Sigma-Aldrich-	Cat#MAK362
Clarity Western ECL substrate	Bio-Rad	Cat#170-5061
Complex I Enzyme Activity Assay Kit	Abcam	Cat#ab109721
DNase I, amplification Grade	Invitrogen (ThermoFischer)	Cat#18068015
GOT/AST IFCC. Enzymatic - UV	Spinreact	Cat#41270
GPT/ALT IFCC. Enzymatic - UV	Spinreact	Cat#41280
IL-6 Mouse ELISA kit	Invitrogen™	Cat#KMC0061
<i>In situ</i> cell death detection kit	Roche	Cat#11684795910
Micro BCA Protein Assay Kit	Thermo Fisher Scientific	Cat#23235
MitoSOXTM Red Mitochondrial Superoxide Indicator	Invitrogen (ThermoFischer)	Cat#M36008
MitoTracker™ Green FM	Invitrogen (ThermoFischer)	Cat#M7514
M-MLV Reverse Transcriptase (200 U/mL)	Invitrogen (ThermoFischer)	Cat#28025013
NAD/NADH Assay Kit	Abcam	Cat#ab65348
NEDD8 mouse ELISA kit	MyBiosource	Cat#MBS109530
NeutrAvidin-Agarose beads	ThermoScientific	Cat#29200

(Continued on next page)

Continued

REAGENT or RESOURCE	SOURCE	IDENTIFIER
Pre-equilibrated PD10 columns	GE Healthcare	Cat#28-9232-45
Protein A/G PLUS-Agarose	Santa Cruz Biotechnology	Cat#2003
Protein Assay Dye Reagent Concentrate (Bradford)	Bio-Rad	Cat#500-0006
Protein G Sepharose 4 Fast Flow	Cytiva	Cat#GE17-0618-01
Purified Mouse IgG1, κ Isotype Control	BD Pharmingen	Cat#557273
SDH Activity Assay Kit	Merck	Cat#MAK197
SYBRSelect Master Mix	Applied Biosystems (ThermoFischer)	Cat#t44720903
Tetramethylrhodamine Ethyl Ester Perchlorate (TMRE)	ThermoFisher Scientific	Cat#T669
Tumor Necrosis Factor (TNF) ELISA Assay DuoSet II kit	R&D Systems	Cat#DY410
TUNEL Assay Kit – HRP – DAB	Abcam	Cat#ab206386
Vector Vip DAB substrate	Vectorlabs	Cat#SK-4105
Vector Vip purple substrate	Vectorlabs	Cat#SK-4600
Experimental models: Cell lines		
Mice primary hepatocytes	Charles River Laboratories	C57BL/6NCtrl
Experimental models: Organisms/strains		
C57BL/6 mouse	Charles River Laboratories	C57BL/6NCtrl
^{Bio} NEDD8 transgenic mice	CIC bioGUNE animal facility	C57Bl6xCBA F1
^{Bio} UB transgenic mice	CIC bioGUNE animal facility	C57Bl6xCBA F1
Global 14% Protein Rodent Maintenance diet	Envigo	Cat#2014C
Oligonucleotides		
Primers for qPCR, See Table S2	This paper	N/A
Silencer™ Negative Control No. 1 siRNA	Ambion (ThermoFischer)	Cat# 4404021
siTam41 (Fw 5'-GUCUGUGAUUUUAU AGUUCAtt-3', Rv 3'-UGAACUAUAA AUCACAGACTt-5')	Ambion (ThermoFischer) <i>In vitro</i>	Cat#4390771
siTam41 (Fw 5'-GGAGAUAGAUAA AAGCCCAAtt-3', Rv 3'-UGGGCUUUUA UCUAUCUCCag-5')	Ambion (ThermoFischer) <i>In vivo</i>	Cat #4457308
Recombinant DNA		
Plasmid: Overexpression of mice Tam41 (NM_026894)	OriGene	Cat#MR212613
Plasmid: Empty vector (pcDNA3.1-(empty)-TAG)	AddGene	Cat#138209
Software and algorithms		
BioRender	Science Suite Inc	https://www.biorender.com RRID:SCR_018361
Image Lab 6.0.1 software	Bio-Rad Laboratories	https://www.bio-rad.com/es-es/product/image-lab-software?ID=KRE6P5E8Z RRID: N/A
ImageJ	NIH	https://imagej.nih.gov/ij/index.html RRID SCR_003070
PEAKS X software	Bioinformatics solutions	https://www.bioinform.com/peaks-studio/ RRID:SCR_022841
Perseus	Max Planck Institute of Biochemistry	https://www.maxquant.org/perseus/ RRID: N/A
Prism 9 GraphPad software	GraphPad software	https://www.graphpad.com/ RRID: SCR_00278

(Continued on next page)

Continued

REAGENT or RESOURCE	SOURCE	IDENTIFIER
Other		
AXIO Imager A1 Manual	Carl Zeiss	N/A
AXIO Imager D1 Upright Fluorescence Microscope	Carl Zeiss	N/A
BEH C18 Column	Waters Corp	Cat#186002350
ChemiDoc Imaging System	Bio-Rad Laboratories	N/A
Cryostate	Leica Biosystems	Cat# CM 1850 UV
Nitrocellulose transfer membrane	ThermoFischer	Cat# LC2009
Precellys Tissue Homogenizer	Bertin Instruments	N/A
Selectra Junio Spinlab 100 analyser	Vital Scientific Spinreact	N/A
Spectra M2	BioNova	N/A
SpeedVacTM	Thermofischer	SPD131DDA
SYNAPT G2 HDMS TOF	Waters Corp	N/A
Thin-layer chromatography (TLC) silica sheets 20 × 20cm	Merck Millipore	Cat#1055530001
TimsTOF Pro with PASEF coupled online to an Evosep ONE	Bruker Daltonics	N/A
Tissue Homogenizer	FasPrep	N/A
Type 50.4 Ti Fixed-Angle Titanium Rotor	Beckman Coulter	Cat#377299
UPLC-MS	N/A	N/A
ViiA 7 Real-Time PCR System	Applied Biosystems (ThermoFischer)	Cat#4453545
Whatman paper 3MM Chr	GE Healthcare	Cat#3030-931
ImageQuant LAS 4000 imaging system	GE Healthcare	N/A

RESOURCE AVAILABILITY

Lead contact

Further information and requests for resources and reagents should be directed to and will be fulfilled by the lead contact, María Luz Martínez-Chantar (mimartinez@cicbiogune.es).

Materials availability

Mouse lines, ^{Bio}NEDD8 and ^{Bio}UBQ, previously generated and used in this study are available upon request to María Luz Martínez-Chantar (mimartinez@cicbiogune.es).

This study did not generate new unique reagents.

Data and code availability

- This paper does not report original code.
- The mass spectrometry data have been deposited to the ProteomeXchange Consortium (<https://proteomecentral.proteomexchange.org>) via the iProX partner repository: PXD053221.
- Any additional information required to reanalyze the data reported in this paper is available from the [lead contact](#) upon request.

EXPERIMENTAL MODEL AND STUDY PARTICIPANT DETAILS

Human samples and clinical information

This research project was performed in accordance with the ethical code of the World Medical Association, the Declaration of Helsinki, and with local and national laws. The Newcastle and North Tyneside Regional Ethics Committee, the Newcastle Academic Health Partners Bioresource (NAHPB), the Newcastle upon Tyne NHS Foundation Trust Research and Development (R&D) department (Reference numbers: 10/H0906/41; NAHPB Project 48; REC12/NE/0395; R&D 6579; Human Tissue Act licence 12534) and Research Ethics Committee of IDIVAL Cantabria (Code 2017.052) approved the study procedures, and a written informed consent was obtained before inclusion in the study of each patient.

A total of 12 liver samples, with an average age of 36 ± 13 years, from 7 male and 5 female patients with severe ALLI (acetaminophen-induced liver injury) which underwent urgent liver transplantation were included in this study (Table S1). The diagnosis of ALLI, established in the Newcastle Hospitals NHS Foundation Trust (Newcastle, England), was based on clinical data, features of liver histology and exclusion of other possible causes of liver injury (viral hepatitis, biliary diseases, alcohol abuse, non-alcoholic fatty liver disease, autoimmune liver diseases, and hereditary diseases). All stated intentional paracetamol ingestion and had detectable paracetamol blood levels after ingestion. Additionally, 4 liver biopsies from organ transplant donors without liver lesions were used as controls for immunostaining analyses. The healthy biopsies samples were obtained from Marqués de Valdecilla University Hospital, Santander. Finally, the immunohistochemical analysis of global Neddylation levels was performed in paraffin-embedded liver tissue $8\mu\text{m}$ sections from 12 ALLI patients and 4 healthy controls.

Preclinical studies and animal maintenance

All procedures were carried out in accordance with the CIC bioGUNE Animal Care and Use Committee and the local authority (Diputación de Bizkaia), under the codes P-CBG-CBBA-0218 and P-CBG-CBBA-1421, respectively, according to the criteria established by the European Union.

The animals used for the experimentation, male three-month-old C57BL/6J wild-type mice were acquired from Charles River Laboratories and accommodated into the AALAC-accredited CIC bioGUNE animal facilities and maintained at $21 \pm 1^\circ\text{C}$, $45 \pm 10\%$ humidity and 12/12h light/dark cycles and fed a standard diet (Harlan Tekland, Envigo #2014C) with water and *ad libitum*.

Mice were starved for 12h and then acetaminophen or APAP (Sigma-Aldrich, Cat# A7085) was given by intraperitoneal injection as a single dose of 360 mg/kg or 600 mg/kg depending on the experiment's objectives which is specified in the figure legend along the manuscript and in the following section.

BioNEDD8 and BioUBIQUITIN (BioUB) transgenic mice model

In the present work, BioNEDD8 and BioUB transgenic mice (C57Bl6xCBA F1) were used to characterize the proteins undergoing these two post-translational modifications during APAP overdose and their modulation after neddylation inhibition. The generation of these BioUB mice has been previously described in.⁵⁰ The BioUB and BioNEDD8 mice have a random genetic insertion of ubiquitin or NEDD8 sequences, respectively, that are conjugated with biotin sequence and BirA enzyme.

Preclinical model of acetaminophen overdose and treatments

Mice fasted for 12 h received a single dose of APAP 360 mg/kg by intraperitoneal injection. After 24 h of APAP overdose mice were randomly divided into two groups: one was administered subcutaneously with 60 mg/kg of MLN4924 (MeDChemExpress, Cat#HY-70062) dissolved in vehicle solution of 2-hydroxypropyl- β -cyclodextrin (Sigma-Aldrich, Cat# H107), and the other group with vehicle solution as it was described in our previous publications.^{12,18} Finally, mice were sacrificed at 48 h after APAP administration. Moreover, the same experiment was performed but MLN4924 was given after 6 h of APAP 360 mg/kg or 600 mg/kg overdose administration and mice were sacrificed at 24h of APAP overdose.

The set of experiments to silence *Tam41 in vivo* was performed in mice fasted for 12h and treated with 360 mg/kg APAP. After 12h of overdose animals were divided into 3 groups ($n = 4$) one administered with the *SiTam41* (5'-GGAGAUAGAUAAAAGCCCAAtt -3', 3'-UGGGCUUUUAUCUAUCUCCag -5') (Thermo Fisher Scientific, Custom, Catalog #4457308), other two with *siCtrl* (ThermoFischer, Cat# 4404021). 250nm of specific *in vivo* siRNA were resuspended in 625 μL of Nuclease-Free Water (Merck, Cat#W4502). Mice received 1.7 mg/kg of specific *in vivo* siRNA complexed with InvivoFectamine 3.0 Reagent (Invitrogen, USA, Cat#IVFs3001) following the manufacturer's instructions and resuspended in sterile PBS through tail vein injection, which allows a specific silencing in the liver.²⁸ Then, two groups (*siTam41* and *SiCtrl*) were treated with 60 mg/kg of MLN4924 after 24h of APAP overdose. Finally, mice were sacrificed at 48 h after APAP administration.

Serum and liver samples were cryopreserved, and part of the liver tissue was maintained in Paraformaldehyde 4% solution in PBS (Santa Cruz, Cat#Sc-281692) or embedded in the OCT Embedding matrix of the frozen section (Pioneer, Cat#PRC/OCT) to further histological studies.

Isolation and culture of primary hepatocytes

Protocol to obtain primary hepatocyte was previously approved by CIC bioGUNE Animal Care and Use Committee and the local authority (Diputación de Bizkaia) according to the criteria established by the European Union. Primary hepatocytes from male three-month-old C57BL/6J wild-type mice acquired from Charles River (St Germain sur l'Arbresle, France) and maintained at the CIC bioGUNE Animal Facilities were isolated by perfusion with Collagenase type IV (Worthington, Cat#LS004188). Briefly, mice were anesthetized with isoflurane inhalator (1.5% isoflurane in O₂; Baxter SL, Cat#NR60378). Following, the abdominal cavity was opened and the catheter was introduced into the vena cava. Liver was perfused with buffer I (1 \times stock solution (Sigma-Aldrich: D-Glucose Cat#G7021, KCl Cat#G7021, NaHCO₃ Cat#S5761 and NaCl Cat#1064041000 from PanReac AppliChem), 5 mM EGTA (Sigma-Aldrich Cat# E3889) (37 °C, oxygenated), and portal vein was cut. Then, liver was washed with buffer II (1 \times stock solution) and subsequently, liver was perfused with buffer III (1 \times stock solution, 2 mM CaCl₂ (Sigma-Aldrich, Cat# C5670), collagenase type I (Worthington) (37 °C, oxygenated). After the perfusion, liver was placed in a Petri dish containing Minimum Essential Medium (MEM; Gibco, #Cat31095029) with 1% penicillin (100 U/ml), streptomycin (100U/ml), Amphotericin (100U/ml) (Anti-Anti; Gibco,

Cat#10378016), glutamine 2 mM (1%) (Gibco, Cat#25030-024) and 10% of fetal bovine serum (FBS; Gibco, Cat#A38401) to stop the collagenase activity and softly disaggregated with forceps. Then, processed liver was filtered over sterile gauze and recollected in a 50 mL Falcon. Subsequently, hepatocytes were centrifugate 48g for 5 min and washed twice with complete media (10% FBS MEM medium supplemented with 1% PSA and 1% Glutamine). Supernatant was discarded and the pellet was resuspended in complete media. Cell viability was validated by trypan blue exclusion test and more than 70% of viability was considered acceptable to proceed with the experiments. Cell density was estimated in a Neubauer counting chamber and the desired density of mouse primary hepatocytes was seeded over collagen I (Corning, Cat#354236) coated 35mm tissue culture dishes (5×10^5 cells/dish) in complete media and maintained in a 5% CO_2 -95% air incubator at 37°C during 6h. After that, medium was replaced for 0% FBS MEM supplemented with 1% PSA and 1% Glutamine overnight and the treatments were performed.

METHOD DETAILS

Hepatocytes transfections and drug treatments

WT primary hepatocytes were transfected with 100 nM of *siTam41* (5'-GUCUGUGAUUUUAGUUCAtt-3', 3'-UGAACUAAAUCA CAGACTt-5') (Ambion; Cat#4390771) or siCtrl (Ambion; Cat# 4404021) using Dharmafect 1 (GE Healthcare Dharmacon, Cat#T-2001-01) following the manufacturer's instructions. For overexpressing Tam41, WT primary hepatocytes were transfected *Tam41* (NM_026894) OriGene (Cat#: MR212613) or with an Empty vector (pcDNA3.1-(empty)-TAG) using jetPRIME (Polyplus, Cat#114-15) according to manufacturer's instructions. Hepatocytes were transfected for 24 h before APAP treatment. Gene knockdown and overexpression were confirmed by RT-PCR.

APAP was dissolved in Dulbecco's Phosphate-Buffered Saline (dPBS 10x, Gibco). Hepatocytes were treated with APAP at a final concentration of 10mM for 1, 3 and 6 h with and without MLN4924 (3 μM).

WT primary hepatocytes were treated with 50 $\mu\text{g/ml}$ cycloheximide (Sigma, Cat#: C1988-1g) with or without MLN4924 (3 μM) and MG132 (Sigma, Cat#: 1211877-36-9) (7 μM) at times of 2, 6, 8, 12 and 24 h.

NEDD8 ELISA assay

Global neddylation levels were analyzed in mice serum samples using NEDD8 ELISA kit (MyBiosource, MBS109530) following manufacturer's instructions.

Interleukin 6 (IL-6) ELISA assay

IL-6 levels were analyzed in serum mice by IL-6 Mouse ELISA kit (Invitrogen KMC0061) following the manufacturer's instructions.

Tumor necrosis factor (TNF) ELISA assay

TNF levels were determined in serum mice by DuoSet II kit (R&D Systems, Cat#DY410) according to manufacturer's protocol.

Cardiolipin assay quantification

Cardiolipin levels were determined in mice liver and in primary isolated mice hepatocytes using Cardiolipin Assay kit (Sigma-Aldrich, MAK362) according to manufacturer's instructions.

Transaminases quantification in serum

Blood samples were obtained by puncture with a heparinized capillary tube in each animal via retroorbital plexus technique. Transaminases were analyzed using a Selectra Junio Spinlab 100 analyser (Vital Scientific, Dieren, The Netherlands) and also using a commercial colorimetric method (Spinreact, Cat# 41270 and 41280) according to the manufacturer's protocol.

Histological procedures

Paraffin-embedded liver samples were sectioned, dewaxed and hydrated. All procedures were performed according to standard protocols using the EnVision+ System HRP (Dako, Cat#K4001). NEDD8 Ubiquitin Like Modifier (NEDD8) staining was performed using 1/200 dilution of NEDD8 antibody (Cell Signaling, #2745) as described previously in.^{15,51} F4/80 staining: was determined as macrophage marker membrane using 1/50 dilution (Bio-Rad, MCA497BB). Proliferating cell nuclear antigen (PCNA) staining was determined using a 1/100 dilution (Santa Cruz Biotechnology, sc-25280) as described in.^{15,51} Samples were incubated with Vector Vip purple substrate (Vectorlabs, #SK-4600) for color development. However, the F4/80 done in Figure S5 was performed using Vector Vip DAB SK-4105 (Vectorlabs, #SK-4105). All the samples were counterstained with Mayer's Haematoxylin (Sigma-Aldrich, Cat# MHS16), dehydrated, cleared in Histo-Clear I solution (Electron Microscopy Science, Cat#64110-004) and mounted with DPX mounting medium (Sigma-Aldrich, Cat#06522). Five to ten random images per sample were taken with an AXIO Imager A1 microscope (Carl Zeiss AG, Jena, Germany). Stained area percentage of each sample were calculated using FIJI (ImageJ) <https://imagej.net/Fiji>.

Hematoxylin and eosin (H&E)

Paraffin-embedded sections of formalin-fixed liver samples were stained for haematoxylin and eosin. Samples were initially deparaffinised in Histo-Clear (Electron Microscopy Sciences) and rehydrated through graded alcohol solutions. After the deparaffinization

and rehydration process, sections were subjected to conventional staining with Harris Hematoxylin (Bio-Optica, Cat#05-06005/L) for 15 min followed by eosin B staining (Sigma Aldrich, Cat#2853) for 15 min. Washed in running tap water for 5 min and differentiated in 0.5% HCl for 1 s. Samples are then dehydrated in graded alcohol solutions until 100% and mounted in DPX mounting medium (Sigma Aldrich). Five to ten random images per sample were taken with an AXIO Imager A1 microscope (Carl Zeiss AG, Jena, Germany). Stained area percentage of each sample were calculated using FIJI (ImageJ) <https://imagej.net/Fiji>.

TUNEL assay for cell death detection *in vitro* cells

Cell death was detected using the *in situ* cell death detection kit (Roche, Cat#11684795910) according to the manufacturer's instructions. Five to ten random images were taken per experimental condition. The percentage of TUNEL positive cells was calculated using FIJI (ImageJ) <https://imagej.net/Fiji>.

TUNEL assay for cell death detection in tissue

TUNEL Assay Kit – HRP – DAB (Abcam, ab206386) was used to determine apoptosis in 5 μ m paraffin-embedded sections of formalin-fixed liver tissue samples following the manufacturer instructions. Five to ten random images were taken per experimental condition. The percentage of TUNEL positive cells was calculated using FIJI (ImageJ) <https://imagej.net/Fiji>.

Dihydroethidium (DHE) staining

To evaluate the oxidative stress present in the liver mice samples the Dihydroethidium fluorescent staining (DHE; Sigma, Cat#D-7008-10mg) was performed in OCT-embeded 8 μ m sections preincubated with MnTBAP 150 μ M 1h at RT. The samples were then incubated with dihydroethidium (DHE) 5 μ M for 30 min at 37°C. Finally, sections were mounted with Fluoromount-G (Southern Biotech, Cat# 0100-01) containing 0.7 mg/L of DAPI to counterstain nuclei.

Streptavidin pull-down assay

Based on the advantages form ^{Bio}UB and ^{Bio}NEDD8 mice that present a biotinylated ubiquitin and NEDD8 *in vivo* respectively, the proteome (Ubiquitinome and NEDDylome) was purified by biotin-streptavidin interaction. The protocol used to capture all the proteins biotinylated in the ^{Bio}NEDD8 transgenic mice was done according to the publication Serrano-Maciá M and Gonzalez-Rellan MJ.^{44,52} Briefly, 250 mg of liver tissue was homogenate with 1.5mL of lysis buffer in denaturing conditions (protease inhibitor cocktail, Roche Cat#11697498001; N-Ethylmaleimide, Sigma-Aldrich Cat#23030). Pre-equilibrated PD10 columns (GE Healthcare, Cat#28-9232-45) were used to clarify the homogenized sample. The elution sample was collected into 15 mL falcon. Then, liver samples were incubated with 250 μ L of NeutrAvidin-Agarose beads (ThermoScientific, Cat#29200), for 1h at room temperature in movement. Next, samples were centrifuged at 2000 rpm for 4 min, and then the supernatant flow through samples were recollected. The beads from each sample were transferred to 1.5 mL Eppendorf tubes in order to perform strict washes with 1 mL of washing buffer 1 (twice), WB2 (thrice), WB3 (once), WB4 (thrice), WB1 (once), WB5 (once), and WB6 (thrice). In order to clean the beads and remove the volume between each washing step, eppendorf were centrifuged at 2000 rpm for 1 min. Finally, beads were mixed with 125 μ L of elution buffer (Boiling buffer 500mM of β -mercapthoethanol (Sigma-Aldrich, Cat#M3148), and 100 mM DTT (Sigma-Aldrich, Cat# DTT-RO) for 10 min in movement, and boiled 95°C for 5 min. A special microcentrifuge filter (VivaClean Mini 0.8 μ L m PES; Sartorius Cat# VK01P042) was used to separate the beads from the elution sample.

Buffer compositions are listed as follows: Lysis buffer contained 8.4 M urea (Sigma-Aldrich, Cat#U5378), 1% SDS (Sigma-Aldrich, Cat#L5750), and 50 mM N-ethylmaleimide in PBS, including a protease inhibitor mixture (Roche Applied Science, Cat#11697498001); binding buffer contained 3 M urea, 1 M NaCl (PanReac AppliChem, Cat#1064041000), 0.25% SDS, and 50 mM N-ethylmaleimide in PBS; WB1 contained 8 M urea and 0.25% SDS in PBS; WB2 contained 6 M guanidine HCl (Sigma-Aldrich, Cat#G3272) in PBS; WB3 contained 6.4 M urea, 1 M NaCl, and 0.2% SDS in PBS; WB4 contained 4.2 M urea, 1 M NaCl, 10% isopropanol (Sigma-Aldrich, Cat#I9516), 10% ethanol (Sigma-Aldrich, Cat#E7023) and 0.2% SDS in PBS; WB5 contained 8 M urea and 1% SDS in PBS; WB6 contained 2% SDS in PBS; and elution buffer contained 4 \times Laemmli buffer and 100 mM DTT.

Protein immunoprecipitation (IP)

NEDD8 was immunoprecipitated from total protein extracts with anti-NEDD8 antibody (ab81264, Abcam) covalently crosslinked to a Protein G Sepharose resin (Cytiva, Cat#GE17-0618-01) to prevent the elution of the antibody with the target protein, as previously described.^{53,54} On the one hand, Protein A/G PLUS-Agarose (Santa Cruz Biotechnology, Cat#2003) was prepared by washing 5 times with 10 column volumes of PBS supplemented with 0.1% sodium azide (Sigma-Aldrich, Cat# S8032) and centrifugation (5,000 rpm, 5 min, 4°C) to remove the storage solution. Beads were resuspended in 0.1% sodium azide-PBS to maintain the initial slurry volume. For each reaction tube, 100 μ L of the Protein A/G PLUS-Agarose slurry were incubated with 2 μ g of NEDD8 antibody (Abcam, Cat#ab81264) or Purified Mouse IgG1, κ Isotype Control antibody (BD Pharmingen, Cat#557273) in a final volume of 1 mL of 0.1% sodium azide-PBS overnight under rotation at 4°C to enable the binding of the antibody to the resin. Next, beads were centrifuged (2,500 rpm, 5 min, 4°C), washed twice with 1 mL of sodium borate buffer (200 mM boric acid, 3 M NaCl, pH 9.0) and incubated with 1 mL of 50 mM dimethyl pimelimidate dihydrochloride (DMP) (Sigma-Aldrich, Cat#80490) dissolved in sodium borate buffer during 30 min under rotation at RT. Beads were centrifuged (2,500 rpm, 5 min, 4°C), washed twice with 1 mL of sodium borate buffer and two more times with 1 mL of 200 mM ethanolamine pH 8.0, before incubation during 2 h under rotation at RT and protected from the

light to quench unreacted DMP. Beads were centrifuged (2,500 rpm, 5 min, 4°C), washed twice with 1 mL of PBS, two more times with 1 mL of 200 mM glycine pH 2.5 and two additional times with 1 mL PBS to remove residual non-crosslinked antibody. On the other hand, cells were collected in 50 mM Tris pH 8.5, 150 mM NaCl, 5 mM EDTA, 1% Igepal lysis buffer (Sigma-Aldrich, Cat#I8896) supplemented with 1 mM phenylmethylsulfonyl fluoride (PMSF, Sigma-Aldrich Cat#52332), and total protein extraction was performed as previously described. Protein concentration of the input fraction was determined by the Micro BCA Protein Assay Kit (Thermo Fisher Scientific, Cat#23235), and 500 μ g of protein were incubated with the antibody crosslinked to the resin in a final volume of 500 μ L of lysis buffer during 2 h under rotation at 4°C. Beads containing the immunoprecipitated proteins were centrifuged (5,000 rpm, 5 min, 4°C) and washed three times with 500 μ L of lysis buffer to remove the unbound material. Samples were incubated with 35 μ L of 4x Laemmli sample loading buffer 5 min under rotation at RT and boiled at 95°C for 5 min to induce protein denaturation and dissociation from the antibody crosslinked to the resin. Samples were eventually centrifuged (13,000 rpm, 12 min, RT) and the supernatant corresponding to the immunoprecipitated protein or elution fraction was submitted to western blotting analysis.

Proteomics analysis by LC-MS/MS

The ubiquitinated and neddylated proteins were extracted from the tissue sample by a Pulldown assay and were analyzed by liquid chromatography-mass spectrometry (LC-MS) as previously described in.^{24,44} Briefly, Samples were analyzed in a timsTOF Pro with PASEF (Bruker Daltonics) coupled online to an Evosep ONE. 200ng of sample were directly loaded in an analytical column (EVOSEP) and resolved at 300 nL/min with a 44 min gradient.

Proteins were identified and quantified by PEAKS X software (Bioinformatics solutions). Searches were performed with a database consisting of *Mus musculus* entries (Uniprot/Swissprot) with precursor and fragment tolerances of 20 ppm and 0.05 Da. Only proteins identified with at least two peptides at FDR <1% were considered for further analysis. Protein abundances derived from PEAKS were loaded onto the Perseus platform⁵⁵ and further log₂-transformed and imputed.

The Database for Annotation, Visualization, and Integrated Discovery (DAVID) was used to elucidate the possible molecular mechanism involved in APAP versus MLN4924 treatment.

Metabolomics analysis

UPLC-MS metabolomics analysis was performed in mice livers (20 mg). Reduced or oxidized glutathione (GSH and GSSG respectively).³⁴ All liver extractions were carried out in the same method with an optimized technique for polar metabolites (GSH and GSSG). In brief, liver tissues were homogenized in 500 mL of ice-cold extraction liquid (EL) contained methanol/water (50/50% v/v) with 10 mM acetic acid (Sigma-aldrich, Cat# 34860 and Cat# W200603) with a tissue homogenizer (FastPrep) in a 40 s cycle at 6000 rpm. Subsequent 400 mL of homogenate was transferred into a new aliquot and shaken for 30 min at 1400 rpm and centrifuged for 30 min at 14000 rpm at 4°C. Next, 75 mL of the supernatant was transferred to a fresh aliquot and stored at -80°C for 30 min. The chilled supernatants were evaporated with a speedvac in approximately 2 h. The resulting pellets were resuspended in 250 mL water/acetonitrile (MeCN; Sigma-aldrich, Cat# 34851)/formic acid (FA; AppliChem #Cat1002641000) (39.9/60/0.1%v/v/v) resuspension liquid (RL). These resuspensions were transferred to glass vials for LCMS analysis.

The LCMS instrumentation consisted of an Acquity-SQD UPLC system coupled to an SYNAPT G2 HDMS Time of Flight mass spectrometer (Waters Corp.). For all performed assays the following MS settings were kept constant. The ion source temperature was 120°C and capillary temperature 450°C. The flow of the cone and desolvation gas (both nitrogen) were set to 5 L/h and 600 L/h, respectively. A 2 ng/mL leucine-enkephalin solution in RL was infused at 10 mL/min and used for a lock mass to automatically correct deviations in mass accuracy. This signal was measured approximately each 30 s for 0.5 s. Metabolites from the polar set were separated prior to MS analysis under the following conditions. Chromatography was performed on a 2.1 3 100 mm, 1.7 mm BEH amide column (Waters Corp.), thermostated at 40°C. Mobile phase solvent A (aqueous phase) contained 99.5% water, 0.5% FA and 20mM ammonium formate while solvent B (organic phase) contained 29.5% water, 70% MeCN, 0.5% FA and 1 mM ammonium formate. In order to obtain a good separation of the analytes, the following gradient was used: from 5% A to 50% A in 2.4 min in curved gradient (#8, as defined by Waters), from 50% A to 99.9% A in 0.2 min constant at 99.9% A for 1.2 min, back to 5% A in 0.2 min. The flow rate was 0.250 mL/min and the injection volume was 2 mL. All samples were injected randomly. After every 8 injections a QC low and QC high were injected. All samples were injected in duplicate. The MS was operated in positive electrospray ionization (+ESI) in full scan mode for glutathione analysis. The cone voltage was 25 V and capillary voltage was 250 V in +ESI.

Extracted ion traces (XICs) were obtained and integrated for specific analytes in a 20 mDa integration window and subsequently smoothed and integrated with QuanLynx software (Waters Corp.). For GSH the XIC was determined at an m/z = 308.0916 and for GSSG at m/z = 613.1598.

Lipid quantification

Lipid quantification was performed as described.⁵⁶ Briefly, pieces of liver (30 mg) were homogenized in 10 volumes of ice-cold saline buffer (PBS) in a Bead Ruptor Homogenizer (OMNI International) according to the manufacturer's instructions for soft tissues. Lipids were extracted from 1 mg of protein according to the Folch method.⁵⁷ For this, a mixture of chloroform and methanol (2:1, v/v) will be used. Then, for total lipid quantification, thin-layer chromatography plates were stained with a solution of 10% CuSO₄ (w/v) in 8% H₃PO₄ (v/v) and an image of the plate was digitized using the ChemiDoc Imaging System (Bio-Rad Laboratories). Quantification was performed with Image Lab 6.0.1 software (Bio-Rad Laboratories).

RNA isolation and quantitative Real-Time PCR (RT-PCR)

Total RNA from liver and WT primary hepatocytes was isolated using Trizol (Invitrogen, Cat#15596026). 1–2 µg of total RNA were treated with DNase (Invitrogen, Cat#18068015) and reverse transcribed into cDNA using M-MLV Reverse Transcriptase (Invitrogen, Cat#28025013) according to manufacturer's instructions. Quantitative real-time PCR (RT-PCR) was performed using SYBR Select Master Mix (Applied Biosystems, Cat#44720903) and the Viia 7 Real-Time PCR System (Applied Biosystems). The Ct values were normalized to the housekeeping expression (*Arp* or *Gapdh*). Primers sequences are described in Table S2.

Protein isolation and western blotting

Protein extraction from liver tissue or primary hepatocytes were performed in RIPA lysis buffer (1.6 mM Na₂HPO₄, 8.4 mM NaH₂PO₄, 0.1 M NaCl, 0.1% SDS, 0.1% Triton X-100) supplemented with 10 mM sodium deoxycholate (Sigma-Aldrich, Cat# 30970), 1 mM sodium orthovanadate (Sigma-Aldrich, Cat#S6508), 50 mM NaF (Sigma-Aldrich, Cat#S7920), protease (P8340, Sigma-Aldrich) and phosphatase inhibitor cocktails (P2850, Sigma-Aldrich), in addition to 10 mM N-ethylmaleimide (NEM; Sigma-Aldrich, Cat#23030) and 10 mM iodoacetamide (IAA; Sigma-Aldrich, Cat# I6125) cysteine protease inhibitors (prevent non-specific deNEDDylation). Total protein concentration was valued by the Micro BCA Protein Assay Kit (Thermo Fisher Scientific, Cat#23235) using a BSA standard curve, in a SpectraMax M2/M2e microplate reader (Molecular Devices).

For western blotting analysis, 20 µg of total protein were combined with 5x Laemmli sample loading buffer (250 mM Tris pH 6.8, 10% SDS, 50% glycerol, 500 mM β-mercaptoethanol, bromophenol blue), boiled at 95° for 10 min, resolved in Sodium Dodecyl Sulphate-polyacrylamide (SDS-page) gels and transferred in to nitrocellulose membranes (ThermoFischer, Cat# LC2009) using a Trans-Blot Cell electroblotting system (Bio-Rad). The presence of total protein in nitrocellulose membrane was detected by Ponceau S solution (Sigma-Aldrich, Cat#P7170) staining. Following, membranes were blocked with 0.1% Tween 20 (Sigma-Aldrich, Cat#P9416)-TBS solution containing 5% skimmed milk powder for 1 h at room temperature (RT). Then, primary antibody was incubated 1h RT or overnight at 4°C. After three washes for 10 min, the membranes were incubated with the corresponding HRP-linked secondary antibody for 1 h at RT. Subsequently, membranes were washed three times and the Clarity Western ECL substrate (Bio-Rad, Cat#170–5061) was added. The chemiluminescent signal was detected in the ImageQuant LAS 4000 imaging system (GE Healthcare). The antibodies and conditions used for Western Blotting are described in Table S3.

Determination of mitochondrial reactive oxygen species (ROS)

Mitochondrial ROS production in primary hepatocytes was evaluated using MitoSOX Red mitochondrial superoxide indicator (Invitrogen, Cat#M36008) as described previously in.^{51,58} The cells were loaded with 2 mM MitoSOX Red for 10 min at 37°C in a CO₂ incubator. The covers with cells were washed three times with PBS, fixed with Paraformaldehyde 4% for 10 min, and set in a porta with mountain media containing DAPI. Five pictures per experimental condition were acquired randomly using an Axioimager D1 upright fluorescence microscope (Leica Biosystems, Nußloch, Baden-Wurtemberg, Germany). Signal quantification was determined using FIJI (ImageJ) <https://imagej.net/Fiji>.

Mitochondrial labeling

The relative number of functional mitochondria in primary hepatocytes was determined using MitoTracker Green FM (Invitrogen, Cat#M7514) probe as previously described in.^{58,59} The cells were loaded with 100 nM MitoTracker green for 30 min at 37°C in a CO₂ incubator. The covers with cells were washed three times with PBS, fixed with Paraformaldehyde 4% for 10 min, and set in a porta with mountain media containing DAPI. Five pictures per experimental condition were acquired randomly using an Axioimager D1 upright fluorescence microscope. Signal quantification was determined using FIJI (ImageJ) <https://imagej.net/Fiji>.

ATP determination

Extracellular ATP levels in primary hepatocytes were determined by the ATPlite luminescence ATP detection kit (PerkinElmer, Cat#6016943) following manufacturer's instructions. Protein was normalized using the BioRad protein assay. Intracellular ATP levels from primary hepatocytes also were determinate by the the ATPlite luminescence ATP detection kit (PerkinElmer, Cat#6016943) following manufacturer's instructions and levels were normalized by the total protein content.

Cytochrome c oxidase activity measurement in mitochondrial membranes

Cytochrome c oxidases activity measurement in mitochondrial membranes was determined by IMG PHARMA (Derio, Spain). Briefly, the pellet from WT primary hepatocytes was resuspended in 1000 µL of homogenization buffer (250mM Sucrose) and homogenized with Dounce homogenizer (1500 rpm, 15 times). Then, the sample was centrifuged (14000 rpm, 15min, 4°C). Supernatant was discarded. Pellet was resuspended in the homogenization buffer and centrifuged (14000 rpm, 15min, 4°C). The resulting pellet was resuspended in phosphate buffer (0.1M, pH 7.4) and incubated with 3,3'-Diaminobenzidine (DAB; Sigma-Aldrich, Cat#D6815) in presence and absence of cytochrome c. DAB acts as an electron donor by reducing cytochrome c and generating a brown precipitate that is quantified by spectrophotometry (450 nm, every 2 min for 20 min). The rate of the cytochrome c oxidase complex in each sample is determined by using the oxidation of DAB in the linear range.

Determination of the mitochondrial membrane potential

Mitochondrial membrane potential was determined in isolated primary hepatocytes incubated with 0.5 μ M of Tetramethylrhodamine Ethyl Ester Perchlorate (TMRE; ThermoFisher Scientific, Cat#T669) in a CO₂ incubator for 30 min at 37°C. Fluorescence was read at 548 nm (excitation) and 574 nm (emission) using a plate reader Spectra M2 (BioNova).

Succinate dehydrogenase assay kit

Succinate dehydrogenase activity was analyzed in mice liver tissue and primary hepatocytes samples by SDH Activity Assay Kit (Merck, Cat#MAK197) following the manufacturer's instructions.

Complex I Enzyme activity assay kit

Mitochondrial OXPHOS Complex I enzyme activity was analyzed in mice liver tissue and primary hepatocytes samples by Complex I Enzyme Activity Assay Kit (Abcam, ab109721) following the manufacturer's instructions.

NAD⁺/NADH Assay Kit

The quantification of NAD⁺ and NADH, and measure their ratio, was analyzed in mice liver tissue and primary hepatocytes samples by NAD/NADH Assay Kit (Abcam, ab65348) following the manufacturer's instructions.

QUANTIFICATION AND STATISTICAL ANALYSIS

All experiments were performed at least in triplicate, with $n = 4$ *in vitro* and $n = 5$ *in vivo*. Data are expressed as mean \pm SEM for each experimental group. Statistical significance was determined using Prism 9 (GraphPad software, version 9.2.0). Statistical significance was determined by Student's *t* test, when two groups were compared, or one-way analysis of variance ANOVA, when more than two groups were compared, followed by Tukey's range test. A $p < 0.05$ was considered statistically significant. Statistical parameters are given in the figure legends.